3. Northington FJ, Zelaya ME, O'Riordan DP, Blomgren K, Flock DL, Hagberg H *et al.* Failure to complete apoptosis following neonatal hypoxia-ischemia manifests as "continuum" phenotype of cell death and occurs with multiple manifestations of mitochondrial dysfunction in rodent forebrain. *Neuroscience* 2007; **149**: 822–833.
4. Baehrecke EH. Autophagy: dual roles in life and death? *Nat Rev Mol Cell Biol* 2005; **6**: 505–510.
5. Kroemer G, Levine B. Autophagic cell death: the story of a misnomer. *Nat Rev Mol Cell Biol* 2008; **9**: 1004–1010.
6. Berry DL, Baehrecke EH. Growth arrest and autophagy are required for salivary gland cell degradation in Drosophila. *Cell* 2007; **131**: 1137–1148.
7. Hou YC, Chittaranjan S, Barbosa SG, McCall K, Gorski SM. Effector caspase Dcp-1 and IAP protein Bruce regulate starvation-induced autophagy during Drosophila melanogaster oogenesis. *J Cell Biol* 2008; **182**: 1127–1139.
8. Mohseni N, McMillan SC, Chaudhary R, Mok J, Reed BH. Autophagy promotes caspase-dependent cell death during Drosophila development. *Autophagy* 2009; **5**: 329–338.
9. Nezis IP, Lamark T, Velentzas AD, Rusten TE, Bjorkoy G, Johansen T *et al.* Cell death during Drosophila melanogaster early oogenesis is mediated through autophagy. *Autophagy* 2009; **5**: 298–302.
10. Maiuri MC, Zalckvar E, Kimchi A, Kroemer G. Self-eating and self-killing: crosstalk between autophagy and apoptosis. *Nat Rev Mol Cell Biol* 2007; **8**: 741–752.
11. Boya P, Gonzalez-Polo RA, Casares N, Perfettini JL, Dessen P, Larochette N *et al.* Inhibition of macroautophagy triggers apoptosis. *Mol Cell Biol* 2005; **25**: 1025–1040.
12. Galluzzi L, Vicencio JM, Kepp O, Tasdemir E, Maiuri MC, Kroemer G. To die or not to die: that is the autophagic question. *Curr Mol Med* 2008; **8**: 78–91.
13. Klionsky DJ, Abeliovich H, Agostinis P, Agrawal DK, Aliev G, Askew DS *et al.* Guidelines for the use and interpretation of assays for monitoring autophagy in higher eukaryotes. *Autophagy* 2008; **4**: 151–175.
14. Gavrieli Y, Sherman Y, Ben-Sasson SA. Identification of programmed cell death *in situ* via specific labeling of nuclear DNA fragmentation. *J Cell Biol* 1992; **119**: 493–501.
15. Sloop GD, Roa JC, Delgado AG, Balart JT, Hines III MO, Hill JM. Histologic sectioning produces TUNEL reactivity. A potential cause of false-positive staining. *Arch Pathol Lab Med* 1999; **123**: 529–532.
16. Liang XH, Kleeman LK, Jiang HH, Gordon G, Goldman JE, Berry G *et al.* Protection against fatal Sindbis virus encephalitis by beclin, a novel Bcl-2-interacting protein. *J Virol* 1998; **72**: 8586–8596.
17. Terauchia S, Yamamotoa T, Yamashita K, Kataoka M, Terada H, Shinohara Y. Molecular basis of morphological changes in mitochondrial membrane accompanying induction of permeability transition, as revealed by immuno-electron microscopy. *Mitochondrion* 2005; **5**: 248–254.
18. de Graaf AO, van den Heuvel LP, Dijkman HB, de Abreu RA, Birkenkamp KU, de Witte T *et al.* Bcl-2 prevents loss of mitochondria in CCCP-induced apoptosis. *Exp Cell Res* 2004; **299**: 533–540.
19. de La Motte Rouge T, Galluzzi L, Olaussen KA, Zermati Y, Tasdemir E, Robert T *et al.* A novel epidermal growth factor receptor inhibitor promotes apoptosis in non-small cell lung cancer cells resistant to erlotinib. *Cancer Res* 2007; **67**: 6253–6262.
20. Godlewski MM, Gajkowska B, Lamparska-Przybysz M, Motyl T. Colocalization of BAX with BID and VDAC-1 in nimesulide-induced apoptosis of human colon adenocarcinoma COLO 205 cells. *Anticancer Drugs* 2002; **13**: 1017–1029.
21. Wang XM, Terasaki PI, Rankin Jr GW, Chia D, Zhong HP, Hardy S. A new microcellular cytotoxicity test based on calcein AM release. *Hum Immunol* 1993; **37**: 264–270.
22. Poncet D, Boya P, Metivier D, Zamzami N, Kroemer G. Cytofluorometric quantitation of apoptosis-driven inner mitochondrial membrane permeabilization. *Apoptosis* 2003; **8**: 521–530.
23. Abrams JM, White K, Fessler LI, Steller H. Programmed cell death during Drosophila embryogenesis. *Development* 1993; **117**: 29–43.
24. Arama E, Steller H. Detection of apoptosis by terminal deoxynucleotidyl transferase-mediated dUTP nick-end labeling and acridine orange in Drosophila embryos and adult male gonads. *Nat Protoc* 2006; **1**: 1725–1731.
25. Robu ME, Larson JD, Nasevicius A, Beiraghi S, Brenner C, Farber SA *et al.* p53 activation by knockdown technologies. *PLoS Genet* 2007; **3**: e78.
26. Petit PX, Lecoeur H, Zorn E, Dauguet C, Mignotte B, Gougeon ML. Alterations in mitochondrial structure and function are early events of dexamethasone-induced thymocyte apoptosis. *J Cell Biol* 1995; **130**: 157–167.
27. Galluzzi L, Zamzami N, de La Motte Rouge T, Lemaire C, Brenner C, Kroemer G. Methods for the assessment of mitochondrial membrane permeabilization in apoptosis. *Apoptosis* 2007; **12**: 803–813.
28. Davis WP, Janssen YM, Mossman BT, Taatjes DJ. Simultaneous triple fluorescence detection of mRNA localization, nuclear DNA, and apoptosis in cultured cells using confocal scanning laser microscopy. *Histochem Cell Biol* 1997; **108**: 307–311.
29. Macho A, Decaudin D, Castedo M, Hirsch T, Susin SA, Zamzami N *et al.* Chloromethyl-X-Rosamine is an aldehyde-fixable potential-sensitive fluorochrome for the detection of early apoptosis. *Cytometry* 1996; **25**: 333–340.
30. Szilagyi G, Simon L, Koska P, Telek G, Nagy Z. Visualization of mitochondrial membrane potential and reactive oxygen species via double staining. *Neurosci Lett* 2006; **399**: 206–209.
31. Petronilli V, Miotto G, Canton M, Brini M, Colonna R, Bernardi P *et al.* Transient and long-lasting openings of the mitochondrial permeability transition pore can be monitored directly in intact cells by changes in mitochondrial calcein fluorescence. *Biophys J* 1999; **76**: 725–734.
32. Wolter KG, Hsu YT, Smith CL, Nechushtan A, Xi XG, Youle RJ. Movement of Bax from the cytosol to mitochondria during apoptosis. *J Cell Biol* 1997; **139**: 1281–1292.
33. Poncet D, Larochette N, Pauleau AL, Boya P, Jalil AA, Cartron PF *et al.* An anti-apoptotic viral protein that recruits Bax to mitochondria. *J Biol Chem* 2004; **279**: 22605–22614.
34. Ostenfeld MS, Fehrenbacher N, Hoyer-Hansen M, Thomsen C, Farkas T, Jaattela M. Effective tumor cell death by sigma-2 receptor ligand siramesine involves lysosomal leakage and oxidative stress. *Cancer Res* 2005; **65**: 8975–8983.
35. Groth-Pedersen L, Ostenfeld MS, Hoyer-Hansen M, Nylandsted J, Jaattela M. Vincristine induces dramatic lysosomal changes and sensitizes cancer cells to lysosome-destabilizing siramesine. *Cancer Res* 2007; **67**: 2217–2225.
36. Kroemer G, Jaattela M. Lysosomes and autophagy in cell death control. *Nat Rev Cancer* 2005; **5**: 886–897.
37. Kluck RM, Bossy-Wetzel E, Green DR, Newmeyer DD. The release of cytochrome c from mitochondria: a primary site for Bcl-2 regulation of apoptosis. *Science* 1997; **275**: 1132–1136.
38. Susin SA, Lorenzo HK, Zamzami N, Marzo I, Brenner C, Larochette N *et al.* Mitochondrial release of caspase-2 and -9 during the apoptotic process. *J Exp Med* 1999; **189**: 381–394.
39. Susin SA, Lorenzo HK, Zamzami N, Marzo I, Snow BE, Brothers GM *et al.* Molecular characterization of mitochondrial apoptosis-inducing factor. *Nature* 1999; **397**: 441–446.
40. Criollo A, Galluzzi L, Maiuri MC, Tasdemir E, Lavandero S, Kroemer G. Mitochondrial control of cell death induced by hyperosmotic stress. *Apoptosis* 2007; **12**: 3–18.
41. Goldstein J, Waterhouse N, Juin P, Evan G, Green D. The coordinate release of cytochrome c during apoptosis is rapid, complete and kinetically invariant. *Nat Cell Biol* 2000; **2**: 156–162.
42. Patterson GH, Lippincott-Schwartz J. A photoactivatable GFP for selective photolabeling of proteins and cells. *Science* 2002; **297**: 1873–1877.
43. Berman SB, Chen YB, Qi B, McCaffery JM, Rucker III EB, Goebbels S *et al.* Bcl-xL increases mitochondrial fission, fusion, and biomass in neurons. *J Cell Biol* 2009; **184**: 707–719.
44. Castedo M, Coquelle A, Vivet S, Vitale I, Kauffmann A, Dessen P *et al.* Apoptosis regulation in tetraploid cancer cells. *EMBO J* 2006; **25**: 2584–2595.
45. Tamura Y, Simizu S, Osada H. The phosphorylation status and anti-apoptotic activity of Bcl-2 are regulated by ERK and protein phosphatase 2A on the mitochondria. *FEBS Lett* 2004; **569**: 249–255.
46. Hsu YT, Youle RJ. Bax in murine thymus is a soluble monomeric protein that displays differential detergent-induced conformations. *J Biol Chem* 1998; **273**: 10777–10783.
47. Tajeddine N, Galluzzi L, Kepp O, Hangen E, Morselli E, Senovilla L *et al.* Hierarchical involvement of Bak, VDAC1 and Bax in cisplatin-induced cell death. *Oncogene* 2008; **27**: 4221–4232.
48. Bursch W, Hochegger K, Torok L, Marian B, Ellinger A, Hermann RS. Autophagic and apoptotic types of programmed cell death exhibit different fates of cytoskeletal filaments. *J Cell Sci* 2000; **113** (Pt 7): 1189–1198.
49. Seth R, Yang C, Kaushal V, Shah SV, Kaushal GP. p53-dependent caspase-2 activation in mitochondrial release of apoptosis-inducing factor and its role in renal tubular epithelial cell injury. *J Biol Chem* 2005; **280**: 31230–31239.
50. Galluzzi L, Vitale I, Kepp O, Seror C, Hangen E, Perfettini JL *et al.* Methods to dissect mitochondrial membrane permeabilization in the course of apoptosis. *Methods Enzymol* 2008; **442**: 355–374.
51. Troiano L, Ferraresi R, Lugli E, Nemes E, Roat E, Nasi M *et al.* Multiparametric analysis of cells with different mitochondrial membrane potential during apoptosis by polychromatic flow cytometry. *Nat Protoc* 2007; **2**: 2719–2727.
52. Castedo M, Ferri K, Roumier T, Metivier D, Zamzami N, Kroemer G. Quantitation of mitochondrial alterations associated with apoptosis. *J Immunol Methods* 2002; **265**: 39–47.
53. Zermati Y, Mouhamad S, Stergiou L, Besse B, Galluzzi L, Boehrer S *et al.* Nonapoptotic role for Apaf-1 in the DNA damage checkpoint. *Mol Cell* 2007; **28**: 624–637.
54. Martin SJ, Reutelingsperger CP, McGahon AJ, Rader JA, van Schie RC, LaFace DM *et al.* Early redistribution of plasma membrane phosphatidylserine is a general feature of apoptosis regardless of the initiating stimulus: inhibition by overexpression of Bcl-2 and Abl. *J Exp Med* 1995; **182**: 1545–1556.
55. Komoriya A, Packard BZ, Brown MJ, Wu ML, Henkart PA. Assessment of caspase activities in intact apoptotic thymocytes using cell-permeable fluorogenic caspase substrates. *J Exp Med* 2000; **191**: 1819–1828.
56. Li J, Petrassi HM, Tumanut C, Masick BT, Trussell C, Harris JL. Substrate optimization for monitoring cathepsin C activity in live cells. *Bioorg Med Chem* 2009; **17**: 1064–1070.
57. LeBel CP, Ischiropoulos H, Bondy SC. Evaluation of the probe 2',7'-dichlorofluorescin as an indicator of reactive oxygen species formation and oxidative stress. *Chem Res Toxicol* 1992; **5**: 227–231.
58. Lecoeur H, Langonne A, Baux L, Rebouillat D, Rustin P, Prevost MC *et al.* Real-time flow cytometry analysis of permeability transition in isolated mitochondria. *Exp Cell Res* 2004; **294**: 106–117.
59. Marzo I, Susin SA, Petit PX, Ravagnan L, Brenner C, Larochette N *et al.* Caspases disrupt mitochondrial membrane barrier function. *FEBS Lett* 1998; **427**: 198–202.
60. Lagasse E, Weissman IL. bcl-2 inhibits apoptosis of neutrophils but not their engulfment by macrophages. *J Exp Med* 1994; **179**: 1047–1052.

61. Qu X, Zou Z, Sun Q, Luby-Phelps K, Cheng P, Hogan RN *et al.* Autophagy gene-dependent clearance of apoptotic cells during embryonic development. *Cell* 2007; **128**: 931–946.
62. Bradbury DA, Simmons TD, Slater KJ, Crouch SP. Measurement of the ADP:ATP ratio in human leukaemic cell lines can be used as an indicator of cell viability, necrosis and apoptosis. *J Immunol Methods* 2000; **240**: 79–92.
63. Tasdemir E, Maiuri MC, Galluzzi L, Vitale I, Djavaheri-Mergny M, D'Amelio M *et al.* Regulation of autophagy by cytoplasmic p53. *Nat Cell Biol* 2008; **10**: 676–687.
64. Vitale I, Galluzzi L, Vivet S, Nanty L, Dessen P, Senovilla L *et al.* Inhibition of Chk1 kills tetraploid tumor cells through a p53-dependent pathway. *PLoS ONE* 2007; **2**: e1337.
65. Baize S, Leroy EM, Georges-Courbot MC, Capron M, Lansoud-Soukate J, Debre P *et al.* Defective humoral responses and extensive intravascular apoptosis are associated with fatal outcome in Ebola virus-infected patients. *Nat Med* 1999; **5**: 423–426.
66. Bonfoco E, Krainc D, Ankarcrona M, Nicotera P, Lipton SA. Apoptosis and necrosis: two distinct events induced, respectively, by mild and intense insults with N-methyl-D-aspartate or nitric oxide/superoxide in cortical cell cultures. *Proc Natl Acad Sci USA* 1995; **92**: 7162–7166.
67. Krysko DV, Vanden Berghe T, D'Herde K, Vandenabeele P. Apoptosis and necrosis: detection, discrimination and phagocytosis. *Methods* 2008; **44**: 205–221.
68. Krysko DV, Vanden Berghe T, Parthoens E, D'Herde K, Vandenabeele P. Methods for distinguishing apoptotic from necrotic cells and measuring their clearance. *Methods Enzymol* 2008; **442**: 307–341.
69. Belzacq-Casagrande AS, Martel C, Pertuiset C, Borgne-Sanchez A, Jacotot E, Brenner C. Pharmacological screening and enzymatic assays for apoptosis. *Front Biosci* 2009; **14**: 3550–3562.
70. Blattner JR, He L, Lemasters JJ. Screening assays for the mitochondrial permeability transition using a fluorescence multiwell plate reader. *Anal Biochem* 2001; **295**: 220–226.
71. Tao Y, Zhang P, Girdler F, Frascogna V, Castedo M, Bourhis J *et al.* Enhancement of radiation response in p53-deficient cancer cells by the Aurora-B kinase inhibitor AZD1152. *Oncogene* 2008; **27**: 3244–3255.
72. Wyllie AH. Glucocorticoid-induced thymocyte apoptosis is associated with endogenous endonuclease activation. *Nature* 1980; **284**: 555–556.
73. George TC, Basiji DA, Hall BE, Lynch DH, Ortyn WE, Perry DJ *et al.* Distinguishing modes of cell death using the ImageStream multispectral imaging flow cytometer. *Cytometry A* 2004; **59**: 237–245.
74. Pouliquen D, Bellot G, Guihard G, Fichet P, Meflah K, Vallette FM. Mitochondrial membrane permeabilization produced by PTP, Bax and apoptosis: a 1H-NMR relaxation study. *Cell Death Differ* 2006; **13**: 301–310.
75. Crouser ED, Gadd ME, Julian MW, Huff JE, Broekemeier KM, Robbins KA *et al.* Quantitation of cytochrome c release from rat liver mitochondria. *Anal Biochem* 2003; **317**: 67–75.
76. Patterson SD, Spahr CS, Daugas E, Susin SA, Irinopoulou T, Koehler C *et al.* Mass spectrometric identification of proteins released from mitochondria undergoing permeability transition. *Cell Death Differ* 2000; **7**: 137–144.
77. Obeid M, Tesniere A, Ghiringhelli F, Fimia GM, Apetoh L, Perfettini JL *et al.* Calreticulin exposure dictates the immunogenicity of cancer cell death. *Nat Med* 2007; **13**: 54–61.
78. Galluzzi L, Joza N, Tasdemir E, Maiuri MC, Hengartner M, Abrams JM *et al.* No death without life: vital functions of apoptotic effectors. *Cell Death Differ* 2008; **15**: 1113–1123.
79. Timmer JC, Salvesen GS. Caspase substrates. *Cell Death Differ* 2007; **14**: 66–72.
80. De Maria R, Zeuner A, Eramo A, Domenichelli C, Bonci D, Grignani F *et al.* Negative regulation of erythropoiesis by caspase-mediated cleavage of GATA-1. *Nature* 1999; **401**: 489–493.
81. Zermati Y, Garrido C, Amsellem S, Fishelson S, Bouscary D, Valensi F *et al.* Caspase activation is required for terminal erythroid differentiation. *J Exp Med* 2001; **193**: 247–254.
82. Janicke RU, Sohn D, Schulze-Osthoff K. The dark side of a tumor suppressor: anti-apoptotic p53. *Cell Death Differ* 2008; **15**: 959–976.

blood

2009 113: 1332-1339
Prepublished online Nov 20, 2008;
doi:10.1182/blood-2008-07-167148

Lactadherin and clearance of platelet-derived microvesicles

Swapan K. Dasgupta, Hanan Abdel-Monem, Polly Niravath, Anhquyen Le, Ricardo V. Bellera, Kimberly Langlois, Shigekazu Nagata, Rolando E. Rumbaut and Perumal Thiagarajan

Blood (print ISSN 0006-4971, online ISSN 1528-0020), is published semimonthly by the American Society of Hematology, 1900 M St, NW, Suite 200, Washington DC 20036.

Lactadherin and clearance of platelet-derived microvesicles

*Swapan K. Dasgupta,[1,2] *Hanan Abdel-Monem,[1,2] Polly Niravath,[3] Anhquyen Le,[1,2] Ricardo V. Bellera,[4] Kimberly Langlois,[4] Shigekazu Nagata,[5] Rolando E. Rumbaut,[1,2,4] and Perumal Thiagarajan[1-3]

[1]Michael E. DeBakey VA Medical Center, Houston, TX; Departments of [2]Pathology, [3]Medicine, and [4]Pediatrics, Baylor College of Medicine, Houston, TX; and [5]Department of Genetics, Osaka University Medical School, Osaka, Japan

The transbilayer movement of phosphatidylserine from the inner to the outer leaflet of the membrane bilayer during platelet activation is associated with the release of procoagulant phosphatidylserine-rich small membrane vesicles called platelet-derived microvesicles. We tested the effect of lactadherin, which promotes the phagocytosis of phosphatidylserine-expressing lymphocytes and red blood cells, in the clearance of platelet microvesicles. Platelet-derived microvesicles were labeled with BODIPY-maleimide and incubated with THP-1–derived macrophages. The extent of phagocytosis was quantified by flow cytometry. Lactadherin promoted phagocytosis in a concentration-dependent manner with a half-maximal effect at approximately 5 ng/mL. Lactadherin-deficient mice had increased number of platelet-derived microvesicles in their plasma compared with their wild-type littermates (950 ± 165 vs 4760 ± 650; $P = .02$) and generated 2-fold more thrombin. In addition, splenic macrophages from lactadherin-deficient mice showed decreased capacity to phagocytose platelet-derived microvesicles. In an in vivo model of light/dye-induced endothelial injury/thrombosis in the cremasteric venules, lactadherin-deficient mice had significantly shorter time for occlusion compared with their wild-type littermate controls (5.93 ± 0.43 minutes vs 9.80 ± 1.14 minutes; $P = .01$). These studies show that lactadherin mediates the clearance of phosphatidylserine-expressing platelet-derived microvesicles from the circulation and that a defective clearance can induce a hypercoagulable state. (Blood. 2009;113:1332-1339)

Introduction

In platelets, as in most mammalian cells, anionic phospholipids such as phosphatidylserine are present only in the inner leaflet of the membrane bilayer.[1] During platelet activation, phosphatidylserine moves from the inner to the outer leaflet of the membrane bilayer.[2] The transbilayer movement of phosphatidylserine is responsible for platelet procoagulant activity by providing high-affinity binding sites for the assembly of the prothrombinase and tenase complex.[3,4] Externalization of anionic phospholipids in platelets is accompanied by the release of phosphatidylserine-rich microvesicles.[5,6] These microvesicles are procoagulant and account for the clot-promoting activity of the serum.[7] More recently, in addition to their hemostatic role, platelet-derived microvesicles were shown to stimulate hematopoietic cells[8] and to transfer platelet-specific receptors to the surface of other cells.[9]

Lactadherin, also known as milk fat globule–epidermal growth factor 8 (EGF-8), is a 45-kDa glycoprotein secreted by macrophages.[10,11] Lactadherin contains EGF-like domains at the amino terminus and 2 C-domains at the carboxy terminus that share homology to the phosphatidylserine-binding domains of blood coagulation factors V and VIII.[12,13] Lactadherin binds to apoptotic cells, activated platelets, and phosphatidylserine-expressing red blood cells via the C-domains and anchors them to macrophage integrins via its RGD sequence in the EGF domain.[14-17] We have examined the role of lactadherin in the clearance of phosphatidylserine-rich platelet-derived microvesicles.

Methods

Reagents

Lactadherin was isolated from fresh unhomogenized milk and labeled with fluorescein isothiocyanate (FITC) as described previously.[18] Annexin A5 was isolated as described previously.[19] The carboxy-terminal fragment of human lactadherin (C1C2 fragment) was amplified from a lactadherin cDNA using primers 5′-TTGAATTCCAGTACGTGAGATTGTACCCCACG-3′ and 5′-TTTGCGGCCGCTAACAGCCCAGCAGCTCC-3′. The amplified fragments were digested with *Eco*R1 and *Not*1 and ligated to the bacterial expression vector pET-28. The recombinant fragment was isolated from *Escherichia coli* as described for bovine lactadherin fragment.[20] Generation of monoclonal antibody to lactadherin was previously described.[21] BODIPY (4,4-difluoro-4-bora-3a,4a-diaza-s-indacene)–maleimide was purchased from Invitrogen (Carlsbad, CA). Human thrombin and purified Russell viper venom were purchased from Haematologic Technologies (Essex Junction, VT). Collagen was purchased from Helena Laboratories (Beaumont, TX). Phycoerythrin (PE)–labeled monoclonal anti–human platelet glycoprotein Ib (anti-CD42b) was purchased from Beckman Coulter (Fullerton, CA). PE-labeled murine anti-CD42b antibody was obtained from eBioscience (San Diego, CA).

Mice

All animal protocols were approved by the Institutional Animal Care and Use Committee of Baylor College of Medicine. C57BL/6J mice were purchased from The Jackson Laboratory (Bar Harbor, ME). The generation of lactadherin-deficient mice was described previously.[22] The lactadherin$^{-/-}$ mice were rederived at Baylor College of Medicine in C57BL/6 mice and backcrossed 6 times to C57BL/6 background.

Submitted July 8, 2008; accepted November 5, 2008. Prepublished online as *Blood* First Edition paper, November 20, 2008; DOI 10.1182/blood-2008-07-167148.

The publication costs of this article were defrayed in part by page charge payment. Therefore, and solely to indicate this fact, this article is hereby marked "advertisement" in accordance with 18 USC section 1734.

*S.K.D. and H.A.-M. contributed equally to this study.

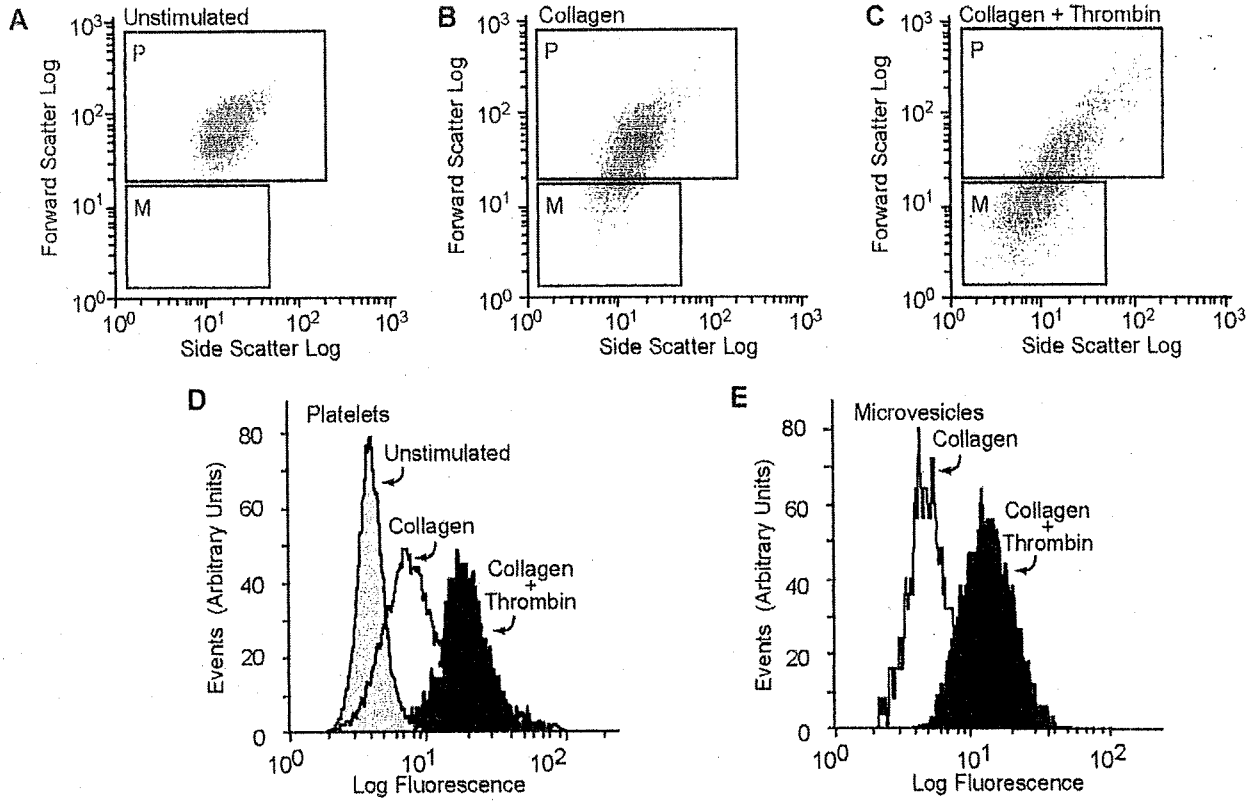

Figure 1. Lactadherin binding to platelets and platelet-derived microvesicles. Washed human platelets were treated with (A) buffer only, (B) collagen (50 μg/mL), or (C) a combination of thrombin (0.1 U/mL) and collagen (50 μg/mL), and FITC-lactadherin (5 μg/mL) and a PE-labeled anti-CD42b (2.5 μg/mL) were added. The generation of microvesicles was analyzed by flow cytometry as described before.[6] To resolve the platelets and platelet-derived microparticles from background scatter, only CD42b$^+$ events were analyzed for forward and side scattering. The gates for microvesicles (gate M) and intact platelets (gate P) were set with the use of isolated microvesicles and unstimulated platelets, respectively. Platelets and microvesicles were analyzed separately for the expression of phosphatidylserine by 5 μg/mL FITC-lactadherin (D,E).

Flow cytometric analysis of lactadherin binding to platelets and platelet-derived microvesicles

Washed platelets were prepared from healthy volunteers after informed consent was obtained in accordance with the Declaration of Helsinki and approved by the Committee for Protection of Human Subjects at Baylor College of Medicine, as described before.[18] Platelets were resuspended in a modified Tyrode buffer[18] containing 1% bovine serum albumin and 1 mM $CaCl_2$. They were activated with collagen (50 μg/mL) or a combination of thrombin (0.1 U/mL) and collagen (50 μg/mL) for 20 minutes at room temperature. FITC-lactadherin (5 μg/mL) and a PE-labeled anti-CD42b (2.5 μg/mL) were added and incubated for 30 minutes at room temperature. Aliquots were then analyzed on a flow cytometer (Coulter FCC 500; Beckman Coulter) using the CXP software. The gates for microvesicles and intact platelets were set with the use of isolated microvesicles and unstimulated platelets, respectively. To differentiate platelets and platelet-derived microvesicles from background scatter, CD42b$^+$ events were gated and analyzed for forward and side scattering. The light scatter and fluorescence channels were set at a logarithmic gain (Figure 1). Ten thousand events per sample were acquired to ensure adequate mean fluorescence levels.

Detection of platelet microvesicle-associated lactadherin in normal human plasma

Blood was drawn through 19-gauge needles into polypropylene syringes containing a one-tenth volume of 3.8% trisodium citrate, pH 6.5. The blood was immediately transferred to polypropylene tubes, and the platelet-rich plasma (PRP) was obtained by centrifugation at 1000*g* for 3 minutes at room temperature. The PRP was centrifuged at 5000*g* for 15 minutes at 4°C to obtain platelet-poor plasma (PPP). The PPP was further centrifuged at 20 000*g* for 20 minutes to sediment the microvesicles. The pellet containing microvesicles was suspended in the modified Tyrode buffer for further analysis. The microvesicles were incubated with a PE-labeled anti-CD42b (2.5 μg/mL) and FITC-anti–lactadherin antibody, L688 (5 μg/mL) for 30 minutes at room temperature for flow cytometry.

Detection of microvesicle-bound lactadherin

An aliquot (100 μg in 100 μL) of rabbit polyclonal anti-IIb/IIIa antibody[23] or irrelevant rabbit control antibody was incubated overnight at 4°C with 100 μL Protein A+G agarose beads (Santa Cruz Biotechnology, Santa Cruz, CA) and washed 3 times (10 000*g* for 2 minutes) in HEPES-buffered saline (HBS). The washed beads were incubated overnight at 4°C with 5 mL human PPP, centrifuged, and washed 3 times in HBS. Bound proteins were eluted in 50 μL 1% SDS and centrifuged and subjected to sodium dodecyl sulfate–polyacrylamide gel electrophoresis (SDS-PAGE; 10%), transferred to a PVDF membrane. The blot was incubated with a monoclonal antibody to lactadherin, L688,[17] and developed with a peroxidase-labeled goat anti–mouse antibody (Thermo Scientific, Rockford, IL) using 4-chloro-1-naphthol (0.3 mg/mL) and H_2O_2 (0.03%).

Isolation and labeling of microvesicles

Washed human platelets were incubated with a combination of thrombin (0.1 U/mL) and collagen (50 μg/mL) for 30 minutes and centrifuged at 2000*g* for 15 minutes. The supernatant plasma, which is platelet-free and microvesicle-rich (as determined by flow cytometry), was further centrifuged at 20 000*g* for 20 minutes. The pellet containing microvesicles was resuspended in HBS and incubated with BODIPY-maleimide (2.5 μM) for 20 minutes and washed twice by centrifugation at 20 000*g* for 20 minutes in HBS.

Peripheral blood mononuclear cells were isolated as described previously,[24] and an aliquot of mononuclear cells (10^8/mL) was stimulated with calcium ionophore A23187 (10 μM) for 30 minutes at 37°C with gentle stirring. The cell suspension was centrifuged at 5000*g* for 15 minutes, the pellet was discarded, and the microvesicles were isolated by centrifugation at 20 000*g* for 20 minutes and labeled with BODIPY-maleimide as described for platelet-derived microvesicles. Human umbilical vein endothelial cells were detached with trypsin-EDTA, washed in serum-free tissue-culture medium (RPMI 1640), and stimulated with calcium ionophore A23187 (10 μM) for 30 minutes at 37°C to release microvesicles. The microvesicles were isolated by centrifugation and labeled as described earlier for human platelet-derived microvesicles.

To isolate microvesicles from mouse platelets, blood was drawn in EDTA (5 mM final concentration) from 4-month-old mice under isoflurane anesthesia from the inferior vena cava and diluted with an equal volume of HBS. PRP was obtained by centrifugation at 260*g* for 10 minutes. Prostaglandin E1 (1 μM) was added, and platelets were sedimented by centrifugation at 1000*g* for 10 minutes and washed twice in modified Tyrode buffer as described for human platelets. Platelet suspension was stimulated with calcium ionophore A23187 (10 μM) containing 1.5 mM $CaCl_2$ at 37°C for 1 hour. The suspension was centrifuged at 5000*g* for 10 minutes, and the pellet was discarded. The microvesicles were labeled with BODIPY-maleimide as described earlier. Splenic macrophages were isolated as described before.[24]

Quantitation of microvesicles from mouse blood

Microvesicles in mouse plasma were quantified as described before with some modification.[25] Briefly, mouse PRP was centrifuged at 5000*g* for 10 minutes at room temperature, and the PPP (250 μL) was diluted to 1 mL by adding 750 μL HBS and incubated with PE-labeled anti–mouse CD42b and analyzed by flow cytometry. The microvesicles were gated as described before for human microvesicles. The flow rate was kept at 10 μL/minute and was run for exactly 3 minutes. On the basis of the dilution, rate, and the time of flow, we calculated the number of microvesicles per microliter of plasma.

Phagocytosis assay

Phagocytosis of platelet-derived microvesicles was quantified by the method described by Hoffmeister et al[26] with some modifications. THP-1 cells (ATCC, Manassas, VA) were grown in tissue culture medium (RPMI 1640 containing 10% fetal bovine serum). The cells were washed in serum-free medium, and phorbol 12-myristate 13-acetate (150 ng/mL) was added and plated on 12-well tissue-culture dish (10^6 cells/well) coated with 2% poly 2-hydroxyethyl methacrylate and incubated for 15 minutes at 37°C. BODIPY-labeled microvesicles (~80 μg) were added to the cells and incubated at 37°C for 30 minutes in the presence of various concentrations of lactadherin. THP-1 cells were incubated with 0.05% trypsin-EDTA to promote detachment and to remove any surface-bound platelet-derived microvesicles. The trypsin was neutralized with fetal calf serum, and the cells were washed twice in serum-free medium and incubated with a PE-labeled anti-CD11b monoclonal antibody (5 μg/mL). The THP-1 cells were gated based on PE fluorescence and forward light scatter and were analyzed for BODIPY fluorescence (green). The results were presented as the percentage of green (BODIPY) fluorescence-positive macrophages. The basal level of phagocytosis, in absence of lactadherin, varied from 10% to 25%.

Thrombin generation assay

Blood samples were collected from mice after anesthesia with a "clean" puncture of the inferior vena cava one-tenth volume of 3.8% trisodium citrate, pH 6.5. Blood samples from 5 mice from each group (lactadherin$^{-/-}$ and littermate controls [lactadherin$^{+/+}$]) were pooled, and PRP was obtained by centrifugation at 260*g* for 10 minutes. PPP was obtained from PRP by centrifuging the blood at 5000*g* for 10 minutes. Microvesicle-free plasma was obtained by further centrifuging the plasma

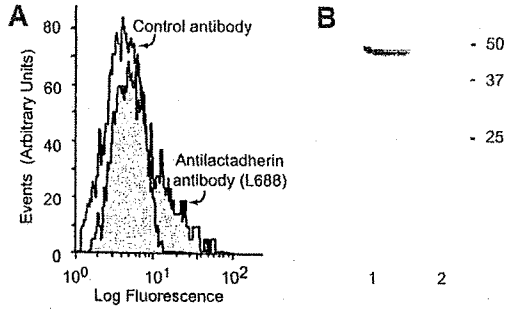

Figure 2. Lactadherin is present in circulating platelet-derived microvesicles in normal human plasma. (A) Microvesicles, isolated from normal human plasma by centrifugation, were incubated with PE-labeled anti-CD42b (2.5 μg/mL) and FITC-antilactadherin antibody L688 (5 μg/mL) or an FITC-labeled irrelevant control antibody. The CD42b-expressing particles were gated and analyzed for FITC fluorescence. (B) Immunoblot of microvesicle-associated lactadherin. Protein A + G agarose beads (100 μL) were incubated overnight at 4°C with 100 μg rabbit polyclonal anti-IIb/IIIa antibody or an irrelevant rabbit control antibody. The beads were washed and incubated with 5 mL platelet-poor plasma and washed. Bound proteins were eluted in 50 μL 1% SDS, subjected to SDS-PAGE, transferred to PVDF membrane, and probed with the monoclonal antibody to lactadherin L688[29] and developed by a peroxidase-labeled goat anti–mouse antibody (1/2000 dilution) and chloronaphthol (0.3 mg/mL) and H_2O_2 (0.03%). (Lane 1) Anti-IIb/IIIa antibody and (lane 2) irrelevant control antibody. (Lane 1) Immunoprecipitation with anti-IIb/IIIa and (lane 2) irrelevant control antibody.

at 20 000*g* for 20 minutes. Thrombin generation in plasma was measured as described before.[27] Briefly, each plasma sample (80 μL) was combined with trigger solution (40 μL) consisting of purified Russell viper venom (3 ng), fluorogenic thrombin substrate Z-Gly-Gly-Arg-AMC (2.5 mM), and $CaCl_2$ (10 mM). The generation of thrombin was measured as a function of fluorescence measured on a fluorimeter over 30 minutes. Thrombin was then quantified by the method described by Hemker et al[27] with the use of an α_2-macroglobulin thrombin complex as standard.

Splenectomy in mice

Mice (4 months old) were anesthetized with an inhalation of isoflurane for the duration of the surgery. After a midline laparotomy, the small bowel was moved to the right of the abdominal cavity and covered with sterile saline. The spleen was approached by dissection, and the splenic blood vessels were tied with Vicryl sutures, and the spleen was removed. The laparotomy was closed in 2 layers with sutures. Four hours later, blood sample was obtained from the inferior vena cava as described earlier.

Mouse model of thrombosis

The in vivo thrombosis was assessed in a mouse model of light/dye-induced endothelial injury as described previously.[28] Mice were anesthetized with an intraperitoneal injection of pentobarbital sodium (50 mg/kg), with additional doses (12.5 mg/kg) as needed. The mice were then placed on a custom Plexiglas tray and maintained at 37°C with a homeothermic blanket and a rectal temperature probe (FHC, Bowdoinham, ME). A tracheotomy was performed to facilitate breathing, and an internal jugular vein and common carotid artery were cannulated for intravenous drug administration and blood pressure/heart rate monitoring, respectively. The cremaster microvascular bed was prepared as described[28] and was superfused continuously with a pH-equilibrated (pH range, 7.35-7.45) bicarbonate-buffered saline solution at 35°C. The preparation was then transferred to the stage of an upright intravital videomicroscope (BX-50; Olympus, Tokyo, Japan) and allowed to equilibrate for 30 minutes. A 4× objective (NA 0.13) lens was used to survey the vascular bed, and a 40× water-immersion objective (NA 0.8) was used to monitor thrombosis kinetics. After a 30-minute equilibration period on the microscope stage, 10 mL/kg 5% FITC-labeled dextran (150 kD) was injected intravenously through the jugular vein. A suitable venule with brisk flow and minimal leukocyte adhesion was selected. After measuring the diameter and blood flow velocity of the vessel

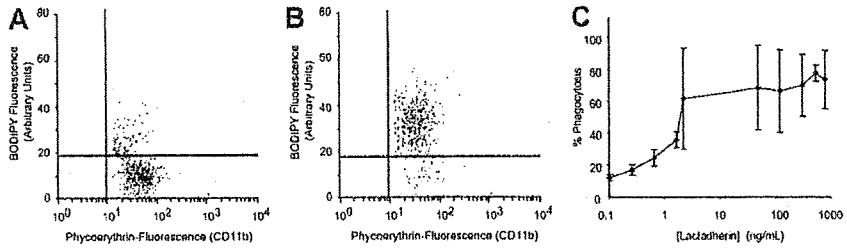

Figure 3. Phagocytosis of platelet-derived microvesicles by macrophages. BODIPY-maleimide–labeled human platelet-derived microvesicles (80 μg) were incubated with THP-1–derived macrophages (10^6 cells/well) for 30 minutes. The nonadherent and the surface-bound microvesicles were detached with trypsin-EDTA solution. The macrophages were washed and analyzed by flow cytometry. The macrophages were identified by PE-labeled CD11b and gated. Phagocytosis was quantified by measuring the percentage of BODIPY (green) fluorescence-positive macrophages. (A) Phagocytosis in the absence of lactadherin. (B) Phagocytosis in the presence of lactadherin (0.8 μg/mL). (C) Lactadherin concentration-dependent phagocytosis of microvesicles. Each point represents the mean and SD of 3 or more separate experiments.

(Doppler velocimeter; Microcirculation Research Institute, College Station, TX), a photochemical injury was started by exposing approximately 100 μm of the vessel to filtered excitation light at 0.6 W/cm^2 (from a 175W xenon lamp; Sutter Instrument, Novato, CA; and an HQ-FITC filter cube; Chroma Technology, Brattleboro, VT).[28,29] Epi-illumination was applied continuously, and the time of onset of platelet aggregates (thrombus onset) and the time of flow cessation (for at least 60 seconds) were recorded. Typically, thrombi were induced in 2 venules per animal, and the results for each animal were averaged.

Statistical analysis

All data are expressed as means and standard deviations of triplicate measurements except when indicated otherwise. Comparisons between individual groups were performed with the use of the Student *t* test with paired and unpaired samples. A probability value (*P*) of .05 or less was considered statistically significant.

Results

Phosphatidylserine expression on platelet microvesicles

Resting washed platelet suspensions had few microparticles (Figure 1A). After activation with collagen, or with a combination of collagen and thrombin, a distinct subpopulation of microvesicles was seen with different light-scattering characteristics (Figure 1A-C) as described before.[6] The expression of phosphatidylserine was measured by FITC-lactadherin binding. FITC-lactadherin binding was increased both in platelets and in microparticle fractions after activation (Figure 1D,E).

Lactadherin is bound to circulating platelet-microvesicles

In normal plasma, platelet-derived microvesicles constitute a major fraction of circulating microvesicles. Because lactadherin is also present in normal plasma,[30] the circulating platelet-derived microvesicles were examined for the presence of lactadherin. Lactadherin is present on the outer surface of platelet-derived microvesicles, as determined by flow cytometry, using a monoclonal antibody to lactadherin L688 (Figure 2A). Lactadherin was also shown in immunoblots of platelet microvesicles, isolated by immunoabsorption with agarose-bound anti–glycoprotein IIb/IIIa antibodies (Figure 2B).

Lactadherin promotes the phagocytosis of microvesicles by macrophages

Differentiated human monocytic THP-1 cells have been used as an in vitro model for phagocytic clearance.[26] When THP-1–derived macrophages were incubated with BODIPY-labeled platelet-derived microvesicles, approximately 10% to 25% of macrophages had phagocytosed platelet-derived microvesicles (Figure 3A). Lactadherin promoted phagocytosis in a concentration-dependent manner with half-maximal effect at approximately 5 ng/mL (Figure

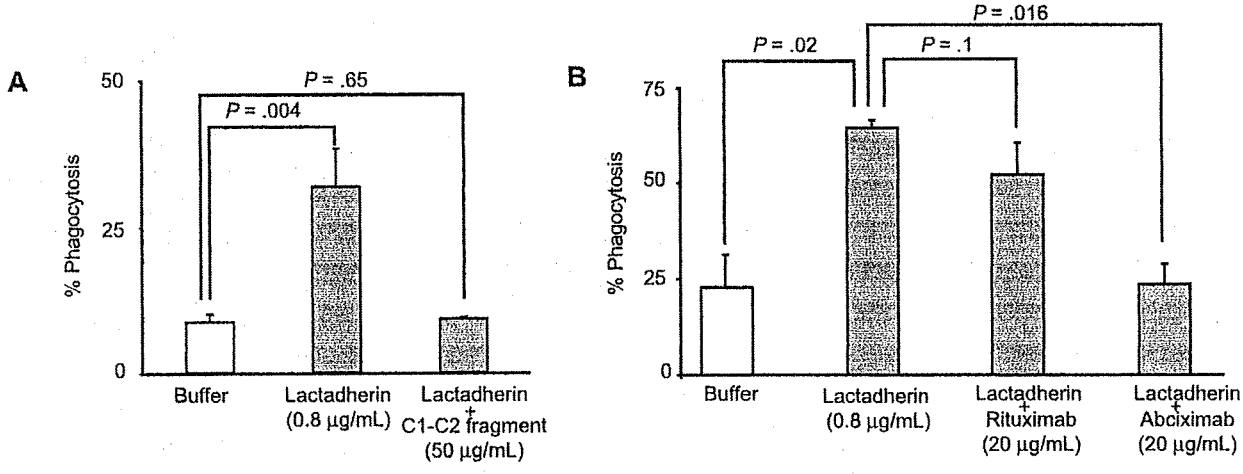

Figure 4. Inhibition of lactadherin-dependent phagocytosis of platelet-derived microvesicles. (A) THP-1–derived macrophages were incubated with BODIPY-labeled human platelet-derived microvesicles and lactadherin in the presence of C1C2 fragment (A) or abciximab (B). The extent of phagocytosis was measured as described in Figure 3. The results are the means and SDs of triplicate measurements.

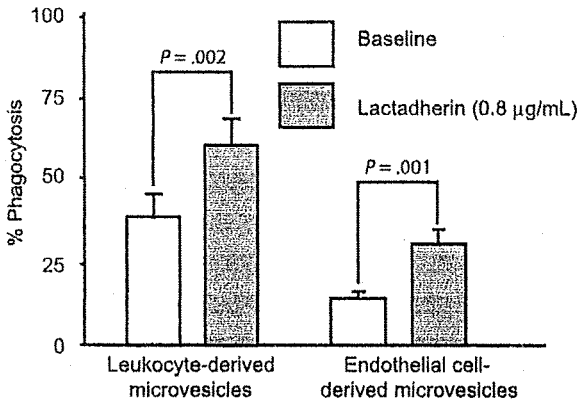

Figure 5. Effect of lactadherin on the phagocytosis of leukocytes and endothelial cell–derived microvesicles. BODIPY-maleimide–labeled microvesicles from peripheral blood leukocytes or human umbilical vein endothelial cells were incubated with THP-1–derived macrophages (10^6 cells/well) for 30 minutes with or without lactadherin (0.8 μg/mL), and the extent of phagocytosis was quantified by flow cytometry by measuring the percentage of green fluorescence (BODIPY)–positive macrophages as in Figure 3.

3B,C). The carboxy-terminal fragment of lactadherin, which has only the phosphatidylserine binding domain (but not the integrin binding domain), inhibited lactadherin-dependent phagocytosis of platelet-derived microvesicles (Figure 4A). Because lactadherin-dependent phagocytosis is mediated by integrins,[10] we examined the effect of abciximab, a human-mouse hybrid Fab fragment that reacts with integrin β3. Abciximab inhibited lactadherin-dependent phagocytosis to approximately 50%, whereas under similar conditions an irrelevant control antibody had no effect (Figure 4B). The stimulatory effect of lactadherin was also seen for the phagocytosis of leukocyte and endothelial cell–derived microvesicles (Figure 5).

Lactadherin-deficient mice have increased microvesicles in the circulation

To determine whether the in vitro findings have an in vivo significance, we quantified the microvesicles in lactadherin-deficient mice and the wild-type littermates by flow cytometry. Littermate control mice had on, an average, 4257 (± 700) microvesicles/μL of blood (Figure 6). In contrast, lactadherin-deficient mice had 8940 (± 1035) microvesicles/μL ($P = .02$; Figure 6). The platelet-derived microvesicles (as determined by CD42b expression) were increased 5-fold in the lactadherin-deficient mice compared with littermate controls (950 ± 165 vs 4760 ± 650; $P = .02$). We posit that the difference is due to the impaired clearance of phosphatidylserine-expressing microvesicles.

Lactadherin-deficient mice have defective phagocytosis of phosphatidylserine-expressing microvesicles

We further studied the phagocytosis of platelet-derived microvesicles by the splenic macrophages isolated from lactadherin-deficient mice and their littermate controls. The splenic macrophages from lactadherin-deficient mice had decreased phagocytosis of phosphatidylserine-expressing microvesicles compared with the wild-type littermate control macrophages (Figure 7; $P = .006$; $n = 3$). Addition of exogenous lactadherin to lactadherin-deficient macrophages corrected the defect in phagocytosis (Figure 7).

Lactadherin-deficient mice generate significantly more thrombin compared with wild-type littermate controls

To determine whether the increased presence of microvesicles in the plasma of lactadherin-deficient mice is associated with increased procoagulant activity, we measured thrombin generation in their plasma. Plasma from lactadherin-deficient mice generated twice as much thrombin as did their wild-type littermate controls (41.5 nM vs 20.4 nM in 30 min) under similar conditions (Figure 8). The difference between the lactadherin-deficient mice and their wild-type littermates was not present in the supernatant plasma, from which microvesicles had been removed by ultracentrifugation.

Hypercoagulable state in lactadherin-deficient mice

Because microvesicles are increased in lactadherin-deficient mice, and plasma from lactadherin-deficient mice generates more thrombin, we tested in vivo thrombus formation in a light/dye-induced endothelial injury/thrombosis model in cremasteric venules. No significant difference was observed in the initiation time for thrombus formation (0.53 ± 0.07 min vs 0.65 ± 0.17 min; $P = .46$; $n = 9$ in each group) between lactadherin-deficient mice and their wild-type littermate controls (lactadherin$^{+/+}$). However, in lactadherin-deficient mice the time for occlusion was significantly shorter (5.93 ± 0.43 min vs 9.80 ± 1.14 min; $P = .01$; $n = 9$ in each group; Figure 9). Microvascular diameters and wall shear rates did not differ between lactadherin-deficient mice and littermate controls (44.3 ± 1.0 μm vs 44.8 ± 1.3 μm, and 513.7 ± 29.8 sec^{-1} vs 550.6 ± 54.0 sec^{-1}, respectively).

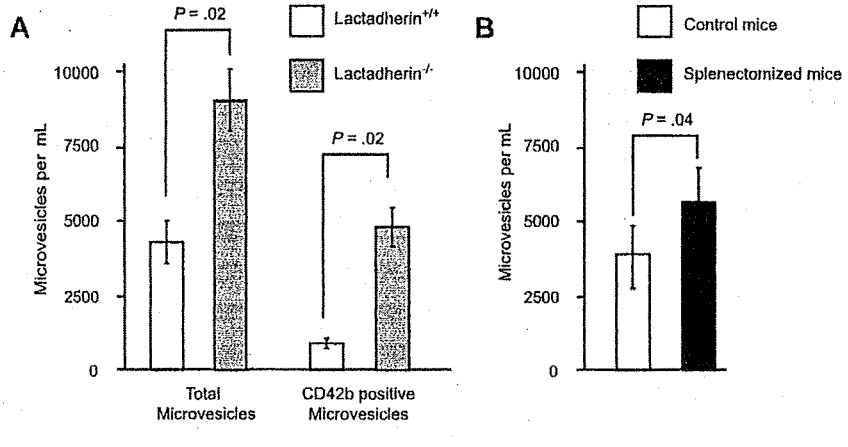

Figure 6. Circulating microvesicles in mouse blood. (A) Plasma was collected from lactadherin-deficient mice and their littermate controls (N = 3 for each group). The microvesicles were quantified by flow cytometry, based on the light scatter and surface expression of CD42b (n = 3). (B) Wild-type mice were subjected to splenectomy, and the circulating microvesicles were measured 4 hours later. The results are the means and SDs (N = 3).

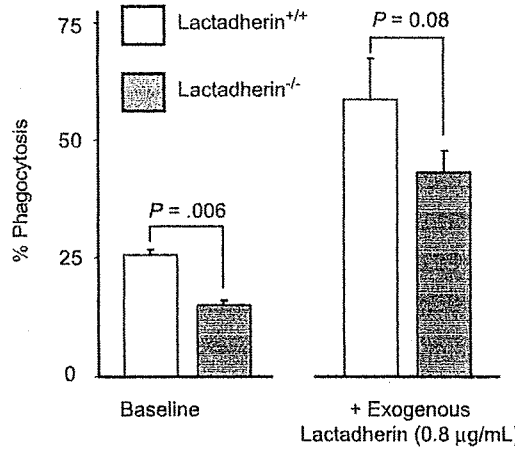

Figure 7. Phagocytosis of platelet-derived microvesicles by splenic macrophages in mice. Splenic macrophages were isolated from lactadherin-deficient mice and their wild-type littermate controls and incubated with BODIPY-labeled mouse platelet-derived microvesicles in the absence or presence of exogenous lactadherin. Phagocytosis of microvesicles was quantified as described before. The results are the means and SDs of triplicate measurements.

Similarly, heart rate and blood pressure did not differ statistically between lactadherin-deficient mice and controls (440.6 ± 24.4 beats/min vs 453.3 ± 15.1 beats/min, and 76.8 ± 4.0 mm Hg vs 68.2 ± 2.2 mm Hg, respectively).

Discussion

The clearance of apoptotic cells by phagocytes is an extremely efficient process. However, even in tissues that are known to contain a large fraction of cells undergoing apoptosis (such as the bone marrow), it is difficult to detect apoptosis by traditional methods, because the apoptotic cells are engulfed rapidly by macrophages.[31] The exposure of phosphatidylserine that occurs during apoptosis is the best-studied macrophage recognition signal, and several receptors have been identified in macrophages that mediate apoptotic cell clearance by binding to phosphatidylserine on apoptotic cells directly or indirectly.[32]

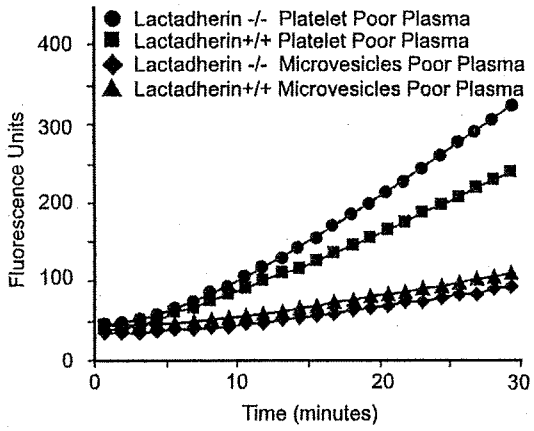

Figure 8. Thrombin generation in the plasma of lactadherin-deficient mice and control littermates. The reaction mixture consisted of plasma (80 μL) and the trigger solution (3 ng purified Russell viper venom in 40 μL), fluorogenic thrombin substrate Z-Gly-Gly-Arg-AMC (2.5 mM), and $CaCl_2$ (10 mM). The generation of thrombin was measured as a function of fluorescence in a fluorimeter over a period of 30 minutes. Thrombin was then calculated using an α_2-macroglobulin thrombin complex standard as described by Hemker et al.[27] Representative data are presented. Blood samples from 5 mice from each group (lactadherin$^{-/-}$ and littermate controls [lactadherin$^{+/+}$]) were pooled for each experiment.

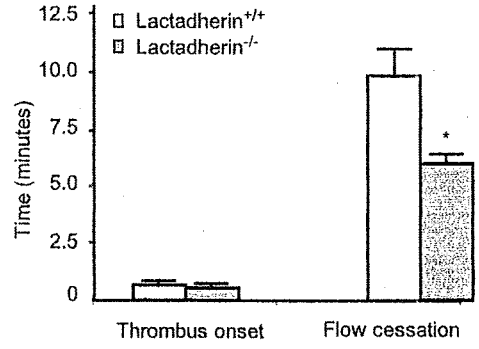

Figure 9. Thrombus formation in lactadherin-deficient mice. Endothelial injury was induced by light/dye in vivo in the cremasteric venules. Thrombus onset and flow cessation were monitored by intravital microscopy in lactadherin-deficient mice (▨) and the littermate controls (□). *P = .01; n = 9.

Platelets lack the machinery to undergo the type of programmed cell death of nucleated cells. However, they appear to have a similar pathway of clearance when activated, involving exposure of phosphatidylserine. Phosphatidylserine is normally located on the cytoplasmic face of the resting platelet membrane. However, after platelet activation with certain agonists that induce sustained increase in intraplatelet calcium such as collagen and shear stress, phosphatidylserine appears on the plasma-oriented surface.[2,4] Externalization of phosphatidylserine in platelet is accompanied by the release of phosphatidylserine-rich microvesicles that are derived from the surface blebs of activated platelets.[6] These microvesicles, initially described as "platelet dusts," are responsible for the clot-promoting activity of plasma.[7] In addition to providing an efficient catalytic surface for prothrombin and factor X activation, microvesicles may have additional hemostatic effects. Microvesicles localize to the subendothelium after vessel wall injury,[33] providing sites for adhesion of platelets and neutrophils.[34] They also improve hemostasis in hemophilic mice.[35] Microvesiculation is defective in Scott syndrome, an inherited bleeding disorder with impaired platelet procoagulant activity resulting from the failure to externalize phosphatidylserine after platelet activation.[36]

Our results show that lactadherin, a macrophage opsonin that mediates the clearance of apoptotic lymphocytes, is one of the mediators of the clearance of phosphatidylserine-expressing procoagulant platelet-derived microvesicles. Platelet-derived microvesicles have a short half-life of less than 5 minutes[37] and must be continuously formed. In an enzyme-linked immunoabsorbent assay assay, we detected approximately 19 plus or minus 1 ng/mL in normal plasma. After centrifugation at 20 000g for 20 minutes, the level decreased to 10 plus or minus 4 ng/mL, suggesting at least 25% of the plasma lactadherin is bound to microvesicles. Lactadherin-deficient mice have increased concentration of microvesicles at steady state, presumably because of their defective clearance, leading to a procoagulant state. The defective phagocytosis by the splenic macrophages from the lactadherin-deficient mice is corrected by exogenous lactadherin. Furthermore, complement-dependent phagocytosis of

zymosan-coated fluorescent particles is normal in lactadherin-deficient mice,[24] indicating no global defect in macrophage function.

Lactadherin competes efficiently with factor V and factor VIII for binding sites on phosphatidylserine with a half-maximal effect at 1 to 4 nM.[38] The procoagulant state seen in lactadherin deficiency could also be due to the absence of natural anticoagulant function of lactadherin. However, increased thrombin is not apparent in microvesicle-poor plasma, suggesting that microvesicles are responsible for the increased thrombin generation. The clearance of phosphatidylserine-containing apoptotic cell surfaces is a fundamental process in development and tissue repair. Therefore, it is not surprising that multiple redundant receptors are involved in their clearance.[31] These receptors are also probably involved in the clearance of platelet-derived microvesicles.

Plasma levels of platelet-derived microvesicles are increased in cancer-associated deep vein thrombosis,[39] antiphospholipid antibody syndrome,[40] disseminated intravascular coagulation, heparin-induced thrombocytopenia,[41] and thrombotic thrombocytopenic purpura,[42] all conditions associated with either arterial and venous thrombosis. The procoagulant microvesicles may have a role in the hypercoagulable state in these conditions. Furthermore, defective clearance of apoptotic cell surfaces is a prominent pathogenetic mechanism in human and murine lupus, and the defective clearance of these vesicles may also play a role in the hypercoagulable state seen in these disorders.

Acknowledgments

This work was supported by grants from the Veterans Affairs Research Service (Washington, DC), the Gulf Coast Regional Blood Center (Houston, TX), and the National Institutes of Health (Bethesda, MD; HL-079368).

Authorship

Contribution: R.E.R. and P.T. designed the experiments; P.N. performed the thrombin generation assay; A.L. cultured the cells and generated the antibodies; R.V.B. and K.L. performed the mouse thrombosis assay; S.N. provided the lactadherin-deficient mice; and S.K.D. and H.A.-M. performed the protein isolation and phagocytosis assay.

Conflict-of-interest disclosure: The authors declare no competing financial interests.

Correspondence: Perumal Thiagarajan, Michael E. DeBakey VA Medical Center, Mail Stop #113, 2002 Holcombe Boulevard, Houston, TX 77030; e-mail perumalt@bcm.tmc.edu.

References

1. Zwaal RF, Comfurius P, Bevers EM. Surface exposure of phosphatidylserine in pathological cells. Cell Mol Life Sci. 2005;62:971-988.
2. Bevers EM, Comfurius P, Zwaal RF. Regulatory mechanisms in maintenance and modulation of transmembrane lipid asymmetry: pathophysiological implications. Lupus. 1996;5:480-487.
3. Zwaal RF, Schroit AJ. Pathophysiologic implications of membrane phospholipid asymmetry in blood cells. Blood. 1997;89:1121-1132.
4. Solum NO. Procoagulant expression in platelets and defects leading to clinical disorders. Arterioscler Thromb Vasc Biol. 1999;19:2841-2846.
5. Comfurius P, Senden JM, Tilly RH, Schroit AJ, Bevers EM, Zwaal RF. Loss of membrane phospholipid asymmetry in platelets and red cells may be associated with calcium-induced shedding of plasma membrane and inhibition of aminophospholipid translocase. Biochim Biophys Acta. 1990;1026:153-160.
6. Sims PJ, Wiedmer T, Esmon CT, Weiss HJ, Shattil SJ. Assembly of the platelet prothrombinase complex is linked to vesiculation of the platelet plasma membrane. Studies in Scott syndrome: an isolated defect in platelet procoagulant activity. J Biol Chem. 1989;264:17049-17057.
7. Wolf P. The nature and significance of platelet products in human plasma. Br J Haematol. 1967; 13:269-288.
8. Baj-Krzyworzeka M, Majka M, Pratico D, et al. Platelet-derived microparticles stimulate proliferation, survival, adhesion, and chemotaxis of hematopoietic cells. Exp Hematol. 2002;30:450-459.
9. Rozmyslowicz T, Majka M, Kijowski J, et al. Platelet- and megakaryocyte-derived microparticles transfer CXCR4 receptor to CXCR4-null cells and make them susceptible to infection by X4-HIV. AIDS. 2003;17:33-42.
10. Hanayama R, Tanaka M, Miwa K, Shinohara A, Iwamatsu A, Nagata S. Identification of a factor that links apoptotic cells to phagocytes. Nature. 2002;417:182-187.
11. Akakura S, Singh S, Spataro M, et al. The opsonin MFG-E8 is a ligand for the alphavbeta5 integrin and triggers DOCK180-dependent Rac1 activation for the phagocytosis of apoptotic cells. Exp Cell Res. 2004;292:403-416.
12. Hvarregaard J, Andersen MH, Berglund L, Rasmussen JT, Petersen TE. Characterization of glycoprotein PAS-6/7 from membranes of bovine milk fat globules. Eur J Biochem. 1996;240:628-636.
13. Andersen MH, Graversen H, Fedosov SN, Petersen TE, Rasmussen JT. Functional analyses of two cellular binding domains of bovine lactadherin. Biochemistry. 2000;39:6200-6206.
14. Asano K, Miwa M, Miwa K, et al. Masking of phosphatidylserine inhibits apoptotic cell engulfment and induces autoantibody production in mice. J Exp Med. 2004;200:459-467.
15. Shi J, Pipe SW, Rasmussen JT, Heegaard CW, Gilbert GE. Lactadherin blocks thrombosis and hemostasis in vivo: correlation with platelet phosphatidylserine exposure. J Thromb Haemost. 2008;6:1167-1174.
16. Shi J, Shi Y, Waehrens LN, Rasmussen JT, Heegaard CW, Gilbert GE. Lactadherin detects early phosphatidylserine exposure on immortalized leukemia cells undergoing programmed cell death. Cytometry A. 2006;69:1193-1201.
17. Dasgupta SK, Thiagarajan P. The role of lactadherin in the phagocytosis of phosphatidylserine-expressing sickle red blood cells by macrophages. Haematologica. 2005;90:1267-1268.
18. Dasgupta SK, Guchhait P, Thiagarajan P. Lactadherin binding and phosphatidylserine expression on cell surface-comparison with annexin A5. Transl Res. 2006;148:19-25.
19. Thiagarajan P, Benedict CR. Inhibition of arterial thrombosis by recombinant annexin V in a rabbit carotid artery injury model. Circulation. 1997;96: 2339-2347.
20. Shao C, Novakovic VA, Head JF, Seaton BA, Gilbert GE. Crystal structure of lactadherin C2 domain at 1.7 angstrom resolution with mutational and computational analyses of its membrane-binding motif. J Biol Chem. 2007;283: 7230-7241.
21. Guchhait P, Dasgupta SK, Le A, Yellapragada S, Lopez JA, Thiagarajan P. Lactadherin mediates sickle cell adhesion to vascular endothelial cells in flowing blood. Haematologica. 2007;92:1266-1267.
22. Hanayama R, Tanaka M, Miyasaka K, et al. Autoimmune disease and impaired uptake of apoptotic cells in MFG-E8-deficient mice. Science. 2004; 304:1147-1150.
23. Thiagarajan P, Shapiro SS, Levine E, DeMarco L, Yalcin A. A monoclonal antibody to human platelet glycoprotein IIIa detects a related protein in cultured human endothelial cells. J Clin Invest. 1985;75:896-901.
24. Dasgupta SK, Abdel-Monem H, Guchhait P, Nagata S, Thiagarajan P. Role of lactadherin in the clearance of phosphatidylserine-expressing red blood cells. Transfusion. 2008;48:2370-2374.
25. Dale GL, Remenyi G, Friese P. Quantitation of microparticles released from coated-platelets. J Thromb Haemost. 2005;3:2081-2088.
26. Hoffmeister KM, Felbinger TW, Falet H, et al. The clearance mechanism of chilled blood platelets. Cell. 2003;112:87-97.
27. Hemker HC, Giesen P, Al Dieri R, et al. Calibrated automated thrombin generation measurement in clotting plasma. Pathophysiol Haemost Thromb. 2003;33:4-15.
28. Rumbaut RE, Randhawa JK, Smith CW, Burns AR. Mouse cremaster venules are predisposed to light/dye-induced thrombosis independent of wall shear rate, CD18, ICAM-1, or P-selectin. Microcirculation. 2004;11:239-247.
29. Rumbaut RE, Sial AJ. Differential phototoxicity of fluorescent dye-labeled albumin conjugates. Microcirculation. 1999;6:205-213.
30. Yamaguchi H, Takagi J, Miyamae T, et al. Milk fat globule EGF factor 8 in the serum of human patients of systemic lupus erythematosus. J Leukoc Biol. 2008;83:1300-1307.
31. Ravichandran KS, Lorenz U. Engulfment of apoptotic cells: signals for a good meal. Nat Rev Immunol. 2007;7:964-974.
32. Fadok VA, Bratton DL, Henson PM. Phagocyte

receptors for apoptotic cells: recognition, uptake, and consequences. J Clin Invest. 2001;108:957-962.

33. Merten M, Pakala R, Thiagarajan P, Benedict CR. Platelet microparticles promote platelet interaction with subendothelial matrix in a glycoprotein IIb/IIIa-dependent mechanism. Circulation. 1999; 99:2577-2582.
34. Forlow SB, McEver RP, Nollert MU. Leukocyte-leukocyte interactions mediated by platelet microparticles under flow. Blood. 2000;95:1317-1323.
35. Hrachovinova I, Cambien B, Hafezi-Moghadam A, et al. Interaction of P-selectin and PSGL-1 generates microparticles that correct hemostasis in a mouse model of hemophilia A. Nat Med. 2003;9:1020-1025.
36. Zwaal RF, Comfurius P, Bevers EM. Scott syndrome, a bleeding disorder caused by defective scrambling of membrane phospholipids. Biochim Biophys Acta. 2004;1636:119-128.
37. Rand ML, Wang H, Bang KW, Packham MA, Freedman J. Rapid clearance of procoagulant platelet-derived microparticles from the circulation of rabbits. J Thromb Haemost. 2006;4: 1621-1623.
38. Shi J, Gilbert GE. Lactadherin inhibits enzyme complexes of blood coagulation by competing for phospholipid-binding sites. Blood. 2003;101: 2628-2636.
39. Tesselaar ME, Romijn FP, Van Der Linden IK, Prins FA, Bertina RM, Osanto S. Microparticle-associated tissue factor activity: a link between cancer and thrombosis? J Thromb Haemost. 2007;5:520-527.
40. Combes V, Simon AC, Grau GE, et al. In vitro generation of endothelial microparticles and possible prothrombotic activity in patients with lupus anticoagulant. J Clin Invest. 1999;104:93-102.
41. Lee DH, Warkentin TE, Denomme GA, Hayward CP, Kelton JG. A diagnostic test for heparin-induced thrombocytopenia: detection of platelet microparticles using flow cytometry. Br J Haematol. 1996;95:724-731.
42. Kelton JG, Warkentin TE, Hayward CP, Murphy WG, Moore JC. Calpain activity in patients with thrombotic thrombocytopenic purpura is associated with platelet microparticles. Blood. 1992;80: 2246-2251.

Cell Death and Differentiation (2009), 1–11

www.nature.com/cdd

Apaf-1-independent programmed cell death in mouse development

A Nagasaka[1,2,5], K Kawane[1,3], H Yoshida[4] and S Nagata*[,1,2,3]

Many cells die during mammalian development and are engulfed by macrophages. In *DNase II*$^{-/-}$ embryos, the TUNEL-positive DNA of apoptotic cells is left undigested in macrophages, providing a system for studying programmed cell death during mouse development. Here, we showed that an *Apaf-1*-null mutation in the *DNase II*$^{-/-}$ embryos greatly reduced the number of macrophages carrying DNA at E11.5. However, at later stages of the embryogenesis, a significant number of macrophages carrying undigested DNA were present in *Apaf-1*$^{-/-}$ embryos, indicating that cells died and were engulfed in an *Apaf-1*-independent manner. In most tissues of the *Apaf-1*$^{-/-}$ embryos, no processed caspase-3 was detected, and the DNA of dead cells accumulated in the macrophages appeared intact. Many nonapoptotic dead cells were found in the tail of the *Apaf-1*$^{-/-}$ embryos, suggesting that the *Apaf-1*-independent programmed cell death occurred, and these dead cells were engulfed by macrophages. In contrast, active caspase-3 was detected in E14.5 thymus of *Apaf-1*$^{-/-}$ embryos. Treatment of fetal thymocytes with staurosporine, but not etoposide, induced processing of procaspases 3 and 9, indicating that the E14.5 thymocytes have the ability to undergo caspase-dependent apoptosis in an *Apaf-1*-independent manner. Thus, programmed cell death in mouse development, which normally proceeds in an efficient Apaf-1-depenent mechanism, appears to be backed up by Apaf-1-independent death systems.
Cell Death and Differentiation advance online publication, 4 December 2009; doi:10.1038/cdd.2009.186

Many useless and toxic cells are generated during animal development and removed by programmed cell death, which is mainly mediated by apoptosis.[1,2] Apoptosis is accompanied by morphological changes, such as the blebbing and condensation of cells, loss of membrane symmetry, and nuclear condensation.[3] Late in apoptosis, dying cells are fragmented into small 'apoptotic bodies,' which are recognized by phagocytes for engulfment. This morphological change in the cells and their rapid disposal are distinct from necrosis, in which cells swell, the plasma membranes are ruptured, and the cellular contents are believed to be released.

The signal transduction involved in apoptotic cell death has been intensively studied[4,5] and shown to proceed by two major pathways, an extrinsic and an intrinsic one. In the extrinsic pathway, signals from death receptors, such as Fas and TNF receptor, activate an initiator caspase, caspase-8, that activates downstream effector caspases, mainly caspase-3, leading to the cleavage of more than 300 cellular proteins.[6,7] One of the caspase-3 substrates is the inhibitor of caspase-activated DNase (CAD), and its cleavage by caspase-3 inactivates the ability to associate with CAD, allowing CAD to cause the fragmentation of chromosomal DNA into nucleosomal units.[8] In the intrinsic pathway, death signals cause the release of cytochrome *c* from mitochondria through 'BH3-only' proteins of the Bcl-2 family.[9,10] The cytochrome *c* binds to Apaf-1 and activates caspase-9, which leads to the activation of caspase-3 and CAD, resulting in the cleavage of cellular substrates and the fragmentation of chromosomal DNA. Apoptotic cells that die by either the intrinsic or the extrinsic pathway expose phosphatidylserine on their surface.[11] Macrophages and immature dendritic cells recognize the phosphatidylserine and rapidly engulf the apoptotic cells.[12] The engulfed dead cells are transferred to lysosomes, where all their components are degraded.

The role of the intrinsic apoptotic pathway in programmed cell death has been studied by establishing mice that lack genes involved in apoptotic signal transduction.[13–17] The results obtained with these knockout mice have not always been consistent among groups. For example, Yoshida *et al.*[14] and Kuida *et al.*[13] reported that Apaf-1 and caspase-9 are indispensable for the cell death induced by cytotoxic agents or γ-radiation in various tissues, whereas Marsden *et al.*[18] reported that lymphocytes undergo apoptosis without Apaf-1 or caspase-9 on cytokine deprivation. Furthermore, except for craniofacial abnormalities and the hyperproliferation of neuronal cells, *Apaf-1*-deficient mice are apparently normal, especially in the C57BL/6 background,[19] suggesting the presence of a back-up system for the Apaf-1-mediated apoptosis in mouse development.

[1]Department of Medical Chemistry, Graduate School of Medicine, Kyoto University, Yoshida-Konoe, Sakyo-ku, Kyoto 606-8501, Japan; [2]Department of Integrated Biology, Graduate School of Frontier Biosciences, Osaka University, 2-2 Yamada-oka, Suita, Osaka 565-0871, Japan; [3]Core Research for Evolutional Science and Technology, Japan Science and Technology Corporation, Yoshida-Konoe, Kyoto 606-8501, Japan and [4]Division of Molecular and Cellular Immunoscience, Department of Biomolecular Sciences, Faculty of Medicine, Saga University, 5-1-1 Nabeshima, Saga 849-8501, Japan
*Corresponding author: S Nagata, Department of Medical Chemistry, Graduate School of Medicine, Kyoto University, Yoshida-Konoe, Sakyo-ku, Kyoto 606-8501, Japan. Tel: +81 75 753 9441; Fax: +81 75 753 9446; E-mail: snagata@mfour.med.kyoto-u.ac.jp
[5]Current address: Tomita Pharmaceutical Co., Akinokami, Seto-cho, Tokushima 771-0306, Japan.
Keywords: apoptosis; caspase; DNase II; macrophage; necrosis; TUNEL
Abbreviations: CAD, caspase-activated DNase; mAb, monoclonal antibody
Received 01.10.09; revised 29.10.09; accepted 04.11.09; Edited by G Melino

Because dying cells are swiftly engulfed and degraded by macrophages, the detection of apoptotic cells in animals is not an easy task. DNase II is responsible for digesting the DNA of apoptotic cells after macrophages engulf them, and many macrophages carrying engulfed DNA are present in *DNase II*-deficient embryos.[20–22] Here, we used *DNase II*-deficient mice to detect the programmed cell death that occurs during mouse development, and found that Apaf-1 seems to be dispensable for this process. In the thymus of *Apaf-1*$^{-/-}$ embryos at E14.5, caspases were activated in an Apaf-1-independent manner. In most other tissues, cells died by an Apaf-1-independent nonapoptotic mechanism, and were engulfed by macrophages. These results indicate that Apaf-1-independent systems, with or without caspase activation, function as back-up systems for the programmed cell death in mammalian development.

Results

Apaf-1-dependent programmed cell death in mouse embryos at E11.5. When we used the TUNEL staining to detect apoptotic cells in E11.5 wild-type mouse embryos, it yielded barely detectable signals (data not shown). A mutation of *nuc-1*, a homologue of *DNase II*, enhances the TUNEL positivity in *C. elegans*.[23] Similarly, the mouse *DNase II*$^{-/-}$ embryos showed very strong TUNEL signals (Figure 1a), which is due to the accumulation of DNA fragmented by CAD.[24] TUNEL-positive spots were frequent in several regions, such as the diencephalon at the cerebrum, the lamina terminalis, somites, and mesonephric ducts. Observations at higher magnification showed TUNEL positivity in these regions was much stronger in the *DNase II*$^{-/-}$ than the wild-type embryos. The TUNEL-positive spots in the *DNase II*$^{-/-}$ embryos were clustered into foci that were strongly DAPI positive (Figure 1b). The foci were located inside F4/80-positive macrophages, suggesting that they were the DNA of engulfed apoptotic cells. The engulfment of corpses in *C. elegans* requires the activation of caspase; a mutation in *Ced-3* or *Ced-4*, homologues of caspase and Apaf-1, respectively, prevents the engulfment of cell corpses.[25] Accordingly, a null mutation of *Apaf-1* blocked the generation of TUNEL-positive foci (Figure 1a and b), indicating that the apoptotic cell death and engulfment of dead cells in the E11.5 mouse embryos were apparently Apaf-1 dependent.

Apaf-1-independent programmed cell death in mouse embryos. Many TUNEL-positive foci were observed throughout the *DNase II*$^{-/-}$ embryos at E14.5 as well (data not shown). *DNase II*$^{-/-}$ embryos produce IFNβ which is lethal, but the lethality can be rescued by a deficiency of IFN type I receptor.[26] To exclude the possible cell death caused by IFNβ, we carried out the TUNEL staining with *DNase II*$^{-/-}$ *IFN-IR*$^{-/-}$ embryos. Many TUNEL-positive foci still could be detected in various tissues of *DNase II*$^{-/-}$*IFN-IR*$^{-/-}$ embryos (Figure 2a ; data not shown), suggesting that the death of the cells in *DNase II*$^{-/-}$ embryos was intrinsic to mouse embryogenesis, and not due to the secondary effect by IFNβ. The null mutation of *Apaf-1* blocked the generation of TUNEL-positive foci in most tissues of the E14.5 *DNase II*$^{-/-}$*IFN-IR*$^{-/-}$ embryos. For example, many TUNEL-positive foci were present at the interdigits of the hind paw of *DNase II*$^{-/-}$*IFN-IR*$^{-/-}$ embryos, and activated caspase-3 could be detected in this region (Figure 2a and b). The deficiency of *Apaf-1* prevented both the caspase activation and the appearance of TUNEL-positive foci. Probably due to the inhibition of apoptotic cell death, the formation of interdigits was retarded in the *Apaf-1*$^{-/-}$*DNase II*$^{-/-}$*IFN-IR*$^{-/-}$ embryos compared with *Apaf-1*$^{+/+}$*DNase II*$^{-/-}$*IFN-IR*$^{-/-}$ embryos, as reported for *Apaf-1*-null mice.[14]

At E17.5, fewer DAPI-positive foci were detected in the *Apaf-1*$^{+/+}$*DNase II*$^{-/-}$*IFN-IR*$^{-/-}$ embryos than at E14.5, as seen, for example, in the interdigits (Figure 2c), which have completely formed by E17.5. In contrast, the interdigits of the *Apaf-1*$^{-/-}$*DNase II*$^{-/-}$*IFN-IR*$^{-/-}$ embryos carried more DAPI-positive foci at E17.5 than at E14.5, and these DAPI-positive materials were located within F4/80-positive macrophages (Figure 2d). Electron microscopy showed that the DNA accumulated in the macrophages at the interdigits of the E17.5 *Apaf-1*$^{+/+}$*DNase II*$^{-/-}$*IFN-IR*$^{-/-}$ embryos is fragmented, whereas the DNA in the *Apaf-1*$^{-/-}$*DNase II*$^{-/-}$*IFN-IR*$^{-/-}$ embryos was apparently intact (Figure 2e). The active caspase-3 could be detected in the interdigits of *Apaf-1*$^{+/+}$ but not *Apaf-1*$^{-/-}$ embryos (data not shown). These results suggested that in late embryogenesis, the cells in the interdigits could die in an Apaf-1-independent manner, and the dead cells were engulfed by macrophages.

Apaf-1-independent nonapoptotic cell death. At the ventral ectodermal ridge of the tail in mouse embryos, many cells undergo programmed cell death, which was detected as DAPI-positive foci in the *DNase II*$^{-/-}$*IFN-IR*$^{-/-}$ embryos at E14.5 (Figure 3a and b). In the *Apaf-1*$^{+/+}$ embryos, the DNA that accumulated in the ridge was TUNEL positive, and many processed caspase-3-positive cells could be detected in this region. On the other hand, the DNA that accumulated in the *Apaf-1*$^{-/-}$ embryos was TUNEL negative, and processed caspase-3-positive cells were hardly detectable. Because the DAPI-positive foci were relatively closely clustered in the ventral ectodermal ridge of the tail (Figure 3c), we analyzed this region by electron microscopy. As shown in Figure 3d, many unengulfed, nonapoptotic dying cells were detected in the E14.5 *Apaf-1*$^{-/-}$ embryos. That is, the unengulfed dying cells showed mottled

Figure 1 Apaf-1-dependent programmed cell death in *DNase II*$^{-/-}$ mouse embryos at E11.5. (a) TUNEL staining of the E11.5 whole embryos. Paraffin sections from E11.5 *Apaf-1*$^{+/-}$*DNase II*$^{-/-}$ and *Apaf-1*$^{-/-}$*DNase II*$^{-/-}$ embryos were stained with TUNEL, followed by counterstaining with methyl green. Scale bar = 500 μm. (b) TUNEL staining of various tissues from E11.5 embryos. Paraffin sections of the diencephalon, lamina terminalis, and somites from E11.5 *Apaf-1*$^{+/-}$*DNase II*$^{+/+}$, *Apaf-1*$^{+/-}$*DNase II*$^{-/-}$, and *Apaf-1*$^{-/-}$*DNase II*$^{-/-}$ embryos, were stained with TUNEL, counterstained with methyl green, and observed by microscopy. For staining of F4/80, cryosections from E11.5 *Apaf-1*$^{+/-}$*DNase II*$^{-/-}$ mouse embryos were stained with DAPI and a rat mAb against mouse F4/80, followed by incubation with peroxidase-conjugated rabbit anti-rat Ig, and detected by Cy3-labeled tyramide. Staining profiles with DAPI and anti-F4/80 are merged, and shown in the middle panels. Polarity of the embryos is indicated in left panels. a, anterior; p, posterior; d, dorsal; v, ventral. Yellow arrowheads indicate the macrophages carrying undigested DNA. Scale bar = 100 μm

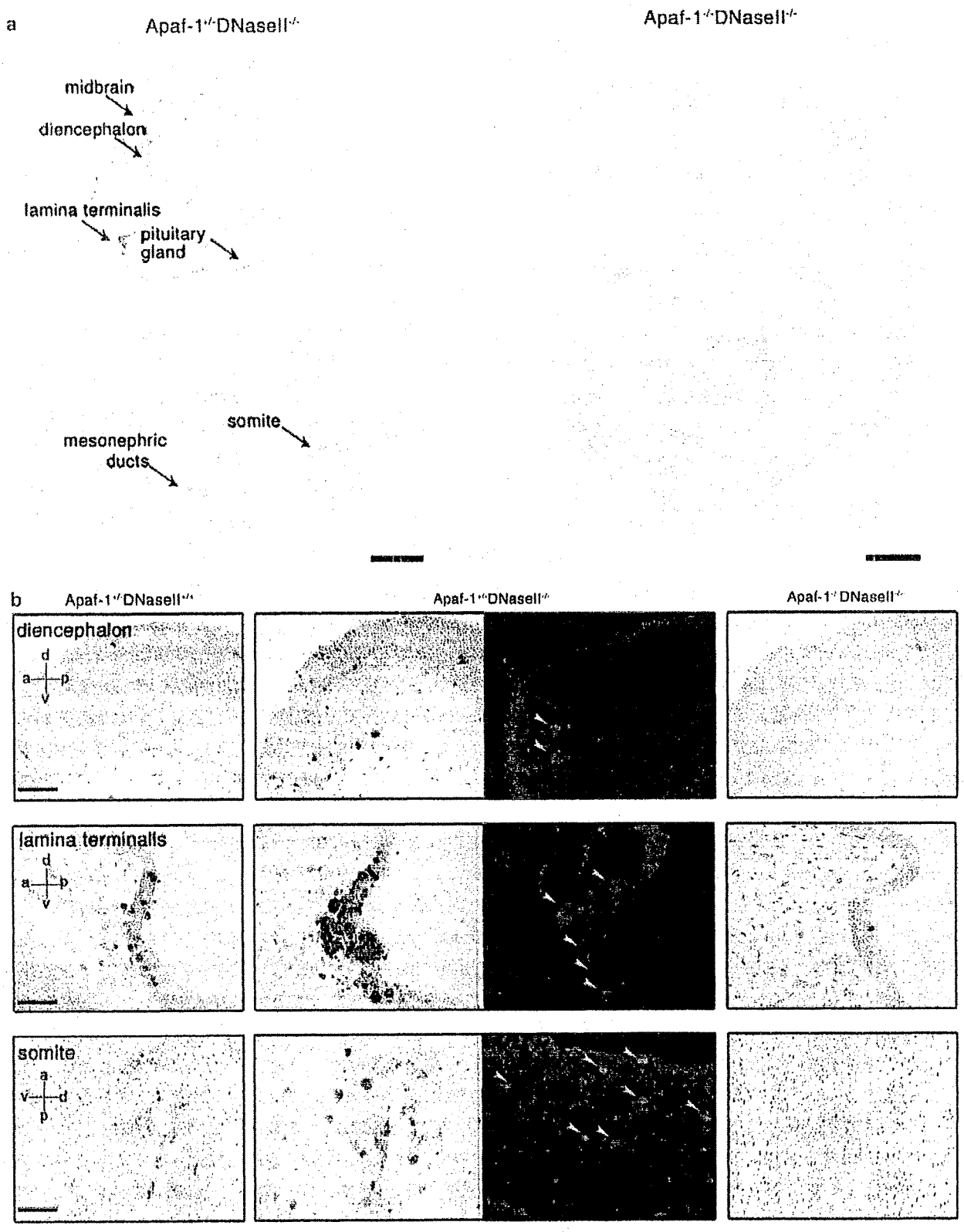
a
Apaf-1-/-DNaseII-/-
Apaf-1-/-DNaseII-/-
midbrain
diencephalon
lamina terminalis
pituitary gland
somite
mesonephric ducts
b
Apaf-1+/+DNaseII+/+
Apaf-1+/-DNaseII-/-
Apaf-1-/-DNaseII-/-
diencephalon
d
a
p
v
lamina terminalis
somite
a
v
d
p

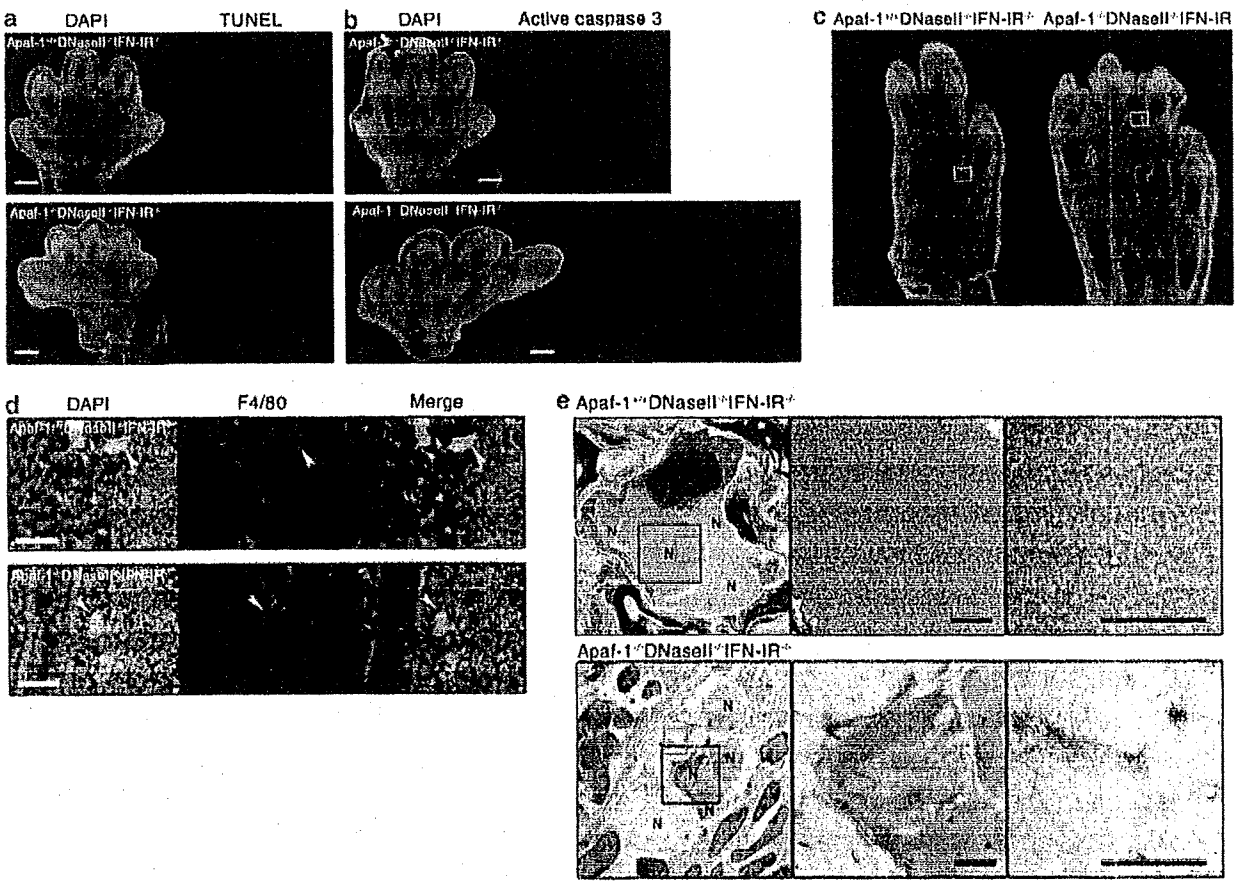

Figure 2 Programmed cell death in the interdigit. (**a** and **b**) Programmed cell death at E14.5. Paraffin sections (**a**) or cryosections (**b**) of the hind paws from E14.5 *Apaf-1*$^{+/+}$ *DNase II*$^{-/-}$ *IFN-IR*$^{-/-}$ (upper) and *Apaf-1*$^{-/-}$ *DNase II*$^{-/-}$ *IFN-IR*$^{-/-}$ (lower) embryos were stained with DAPI and TUNEL (**a**), or with DAPI and an anti-processed caspase-3 mAb (**b**). Scale bar = 100 μm. (**c** and **d**) Programmed cell death at E17.5. Cryosections of the hind paws from E17.5 *Apaf-1*$^{+/+}$ *DNase II*$^{-/-}$ *IFN-IR*$^{-/-}$ (left) and *Apaf-1*$^{-/-}$ *DNase II*$^{-/-}$ *IFN-IR*$^{-/-}$ (right) embryos were stained with DAPI (**c**). The boxed areas in (**c**) are enlarged in (**d**). Sections from E17.5 *Apaf-1*$^{+/+}$ *DNase II*$^{-/-}$ *IFN-IR*$^{-/-}$ (upper) and *Apaf-1*$^{-/-}$ *DNase II*$^{-/-}$ *IFN-IR*$^{-/-}$ (lower) mouse embryos were stained with DAPI and a rat mAb against mouse F4/80, followed by incubation with peroxidase-conjugated rabbit anti-rat Ig, and detected by Cy3-labeled tyramide. The staining profiles with DAPI and anti-F4/80 are merged in the right panels. Arrowheads indicate macrophages carrying engulfed DNA. Scale bars = 50 μm (**d**). (**e**) Electron microscopy. Sections from the E17.5 hind paws of *Apaf-1*$^{+/+}$ *DNase II*$^{-/-}$ *IFN-IR*$^{-/-}$ (upper) and *Apaf-1*$^{-/-}$ *DNase II*$^{-/-}$ *IFN-IR*$^{-/-}$ (lower) mice were analyzed by electron microscopy. Macrophages are indicated by yellow lines. The areas surrounded by black and red boxes are enlarged in the middle and right panels. N, nuclear DNA from the engulfed dead cells. Scale bar = 1 μm

chromatin condensation, nuclear membrane detachment and rupture, and dilated mitochondria. Approximately 5% of the cells in the tail ridge of E14.5 *Apaf-1*$^{-/-}$ embryos had the nonapoptotic morphology (Figure 3e), but apoptotic dying cells were hardly detectable. Nonapoptotic dead cells in the tail ridge of *Apaf-1*$^{+/+}$ embryos were rare, about 1%, but cells with apoptotic characteristics, such as condensed and fragmented nuclei, were relatively abundant (1.72%). These results indicated that the cells in the tail ridge underwent nonapoptotic cell death in the absence of Apaf-1, and that these dead cells were engulfed by macrophages.

Apaf-1-independent apoptosis in the thymus. Many TUNEL- and DAPI-positive foci were observed in the thymus of *DNase II*$^{-/-}$ *IFN-IR*$^{-/-}$ embryos at E14.5 (Figure 4a). In contrast to most other tissues, such as the interdigits and tails at this stage of embryogenesis, the TUNEL-positive foci were present in the *Apaf-1*$^{-/-}$ thymus as well, where processed caspase-3 was also detected. Electron microscopy indicated that the DAPI-positive material in the E14.5 thymus was inside macrophages, and the DNA that accumulated in the macrophages was fragmented in both the *Apaf-1*$^{+/+}$ and the *Apaf-1*$^{-/-}$ thymuses (Figure 4b). These results indicated that the thymocytes at E14.5 could activate caspase-3 and CAD using an Apaf-1-independent mechanism.

The E17.5 *Apaf-1*$^{-/-}$ thymus also carried DAPI-positive foci (Figure 4c). But, in contrast to the E14.5 *Apaf-1*$^{-/-}$ thymus, the TUNEL reactivity of the foci in the E17.5 *Apaf-1*$^{-/-}$ *DNase II*$^{-/-}$ *IFN-IR*$^{-/-}$ thymus was very weak, and processed caspase-3 was barely detected. Staining with F4/80 indicated that the DAPI-positive foci in the *Apaf-1*$^{-/-}$ thymus were inside macrophages (Figure 4c), and the electron microscopy showed that the DNA that accumulated in the macrophages was intact (Figure 4d). These properties of the E17.5 *Apaf-1*$^{-/-}$ thymus were different from those of the E14.5 thymus, but

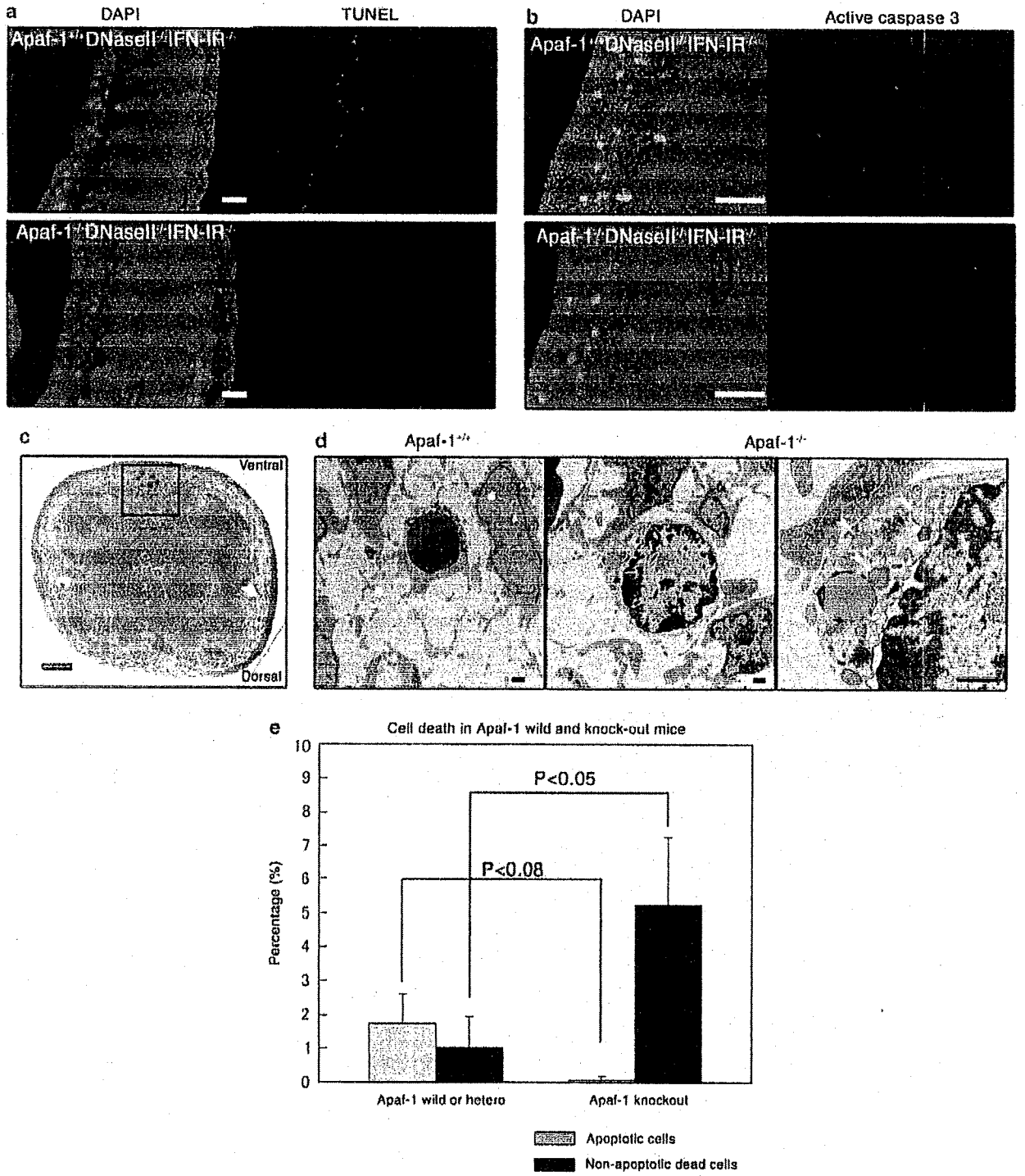

Figure 3 Apaf-1-independent nonapoptotic cell death. (**a–c**) Programmed cell death in the tail. Paraffin sections (**a**) or cryosections (**b**) of the tail from E14.5 *Apaf-1*$^{+/+}$ *DNase II*$^{-/-}$*IFN-IR*$^{-/-}$ (upper) and *Apaf-1*$^{-/-}$*DNase II*$^{-/-}$*IFN-IR*$^{-/-}$ (lower) embryos were stained with DAPI and TUNEL (**a**), and with DAPI and a rabbit mAb against processed caspase-3 (**b**). Scale bar = 100 μm. In (**c**), a transverse section of the tail from an *Apaf-1*$^{+/-}$*DNase II*$^{-/-}$*IFN-IR*$^{-/-}$ embryo at E14.5 was stained with toluidine blue. Scale bars = 100 μm. (**d**) Electron microscopy. Sections from the E14.5 tail of *Apaf-1*$^{+/+}$ *DNase II*$^{+/-}$*IFN-IR*$^{-/-}$ (left) and *Apaf-1*$^{-/-}$*DNase II*$^{+/+}$ *IFN-IR*$^{-/-}$ (middle and right) embryos were analyzed by electron microscopy. Apoptotic cells in the *Apaf-1*$^{+/+}$ embryos (left) and nonapoptotic dead cells (middle and right) in the *Apaf-1*$^{-/-}$ embryos are shown. Arrowheads indicate dilated mitochondria. Scale bar = 1 μm. (**e**) Increase in nonapoptotic dead cells in the *Apaf-1*$^{-/-}$ tail. Electron micrographs (55 × 55 μm) with low magnification of the ventral parts (boxed area in **c**) of the tail of *Apaf-1*$^{+/+}$ or $^{+/-}$ and *Apaf-1*$^{-/-}$ embryos at E14.5 were assembled, and the percentages of apoptotic and nonapoptotic dead cells out of 950 cells were determined. Average numbers obtained from three embryos are plotted

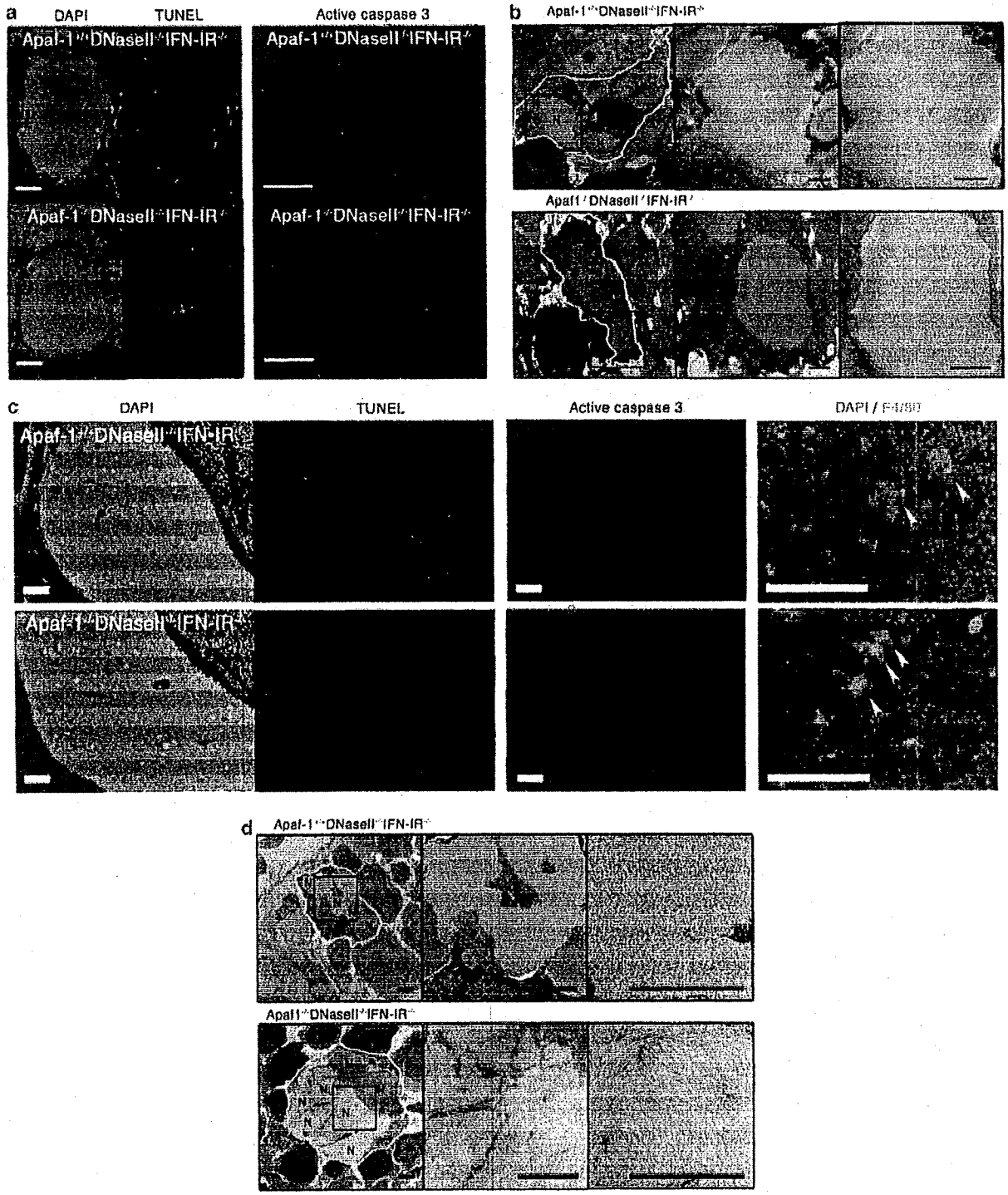

Figure 4 Programmed cell death in the fetal thymus. (**a**) Programmed cell death at E14.5. Paraffin sections (left) or cryosections (right) of the thymus from E14.5 *Apaf-1*$^{+/+}$ *DNase II*$^{-/-}$*IFN-IR*$^{-/-}$ (upper) and *Apaf-1*$^{-/-}$*DNase II*$^{-/-}$*IFN-IR*$^{-/-}$ (lower) embryos were stained with DAPI and TUNEL using the digoxigenin/anti-digoxigenin fluorescein system (left), or with an anti-processed caspase-3 mAb (right). Scale bars = 100 μm. (**b**) Electron microscopy of the E14.5 thymus. Sections from the thymus of E14.5 *Apaf-1*$^{+/+}$ *DNase II*$^{-/-}$*IFN-IR*$^{-/-}$ (upper) and *Apaf-1*$^{-/-}$*DNase II*$^{-/-}$*IFN-IR*$^{-/-}$ (lower) embryos were analyzed by electron microscopy. Boxed areas were enlarged. N, nuclear DNA from the engulfed dead cells; MN, macrophage nuclei. Scale bar = 1 μm. (**c**) Programmed cell death at E17.5. Adjacent cryosections of the thymus from E17.5 embryos with *Apaf-1*$^{+/+}$ *DNase II*$^{-/-}$*IFN-IR*$^{-/-}$ (upper) and *Apaf-1*$^{-/-}$*DNase II*$^{-/-}$*IFN-IR*$^{-/-}$ (lower) embryos were stained with DAPI and TUNEL (left), or with an anti-processed caspase-3 mAb. Scale bars = 100 μm. In the right, the sections were stained with DAPI and a rat mAb against mouse F4/80, and their staining profiles were merged. Yellow arrowheads indicate the macrophages carrying engulfed DNA. Scale bar = 100 μm. (**d**) Electron microscopy of the E17.5 thymus. Sections from the E17.5 thymus of *Apaf-1*$^{+/+}$ *DNase II*$^{-/-}$*IFN-IR*$^{-/-}$ (upper) and *Apaf-1*$^{-/-}$*DNase II*$^{-/-}$*IFN-IR*$^{-/-}$ (lower) embryos were analyzed by electron microscopy. Boxed areas in the left panels were enlarged in the adjacent right panels. N, nuclear DNA from the engulfed dead cells; MN, macrophage nuclei. Scale bars = 2 μm

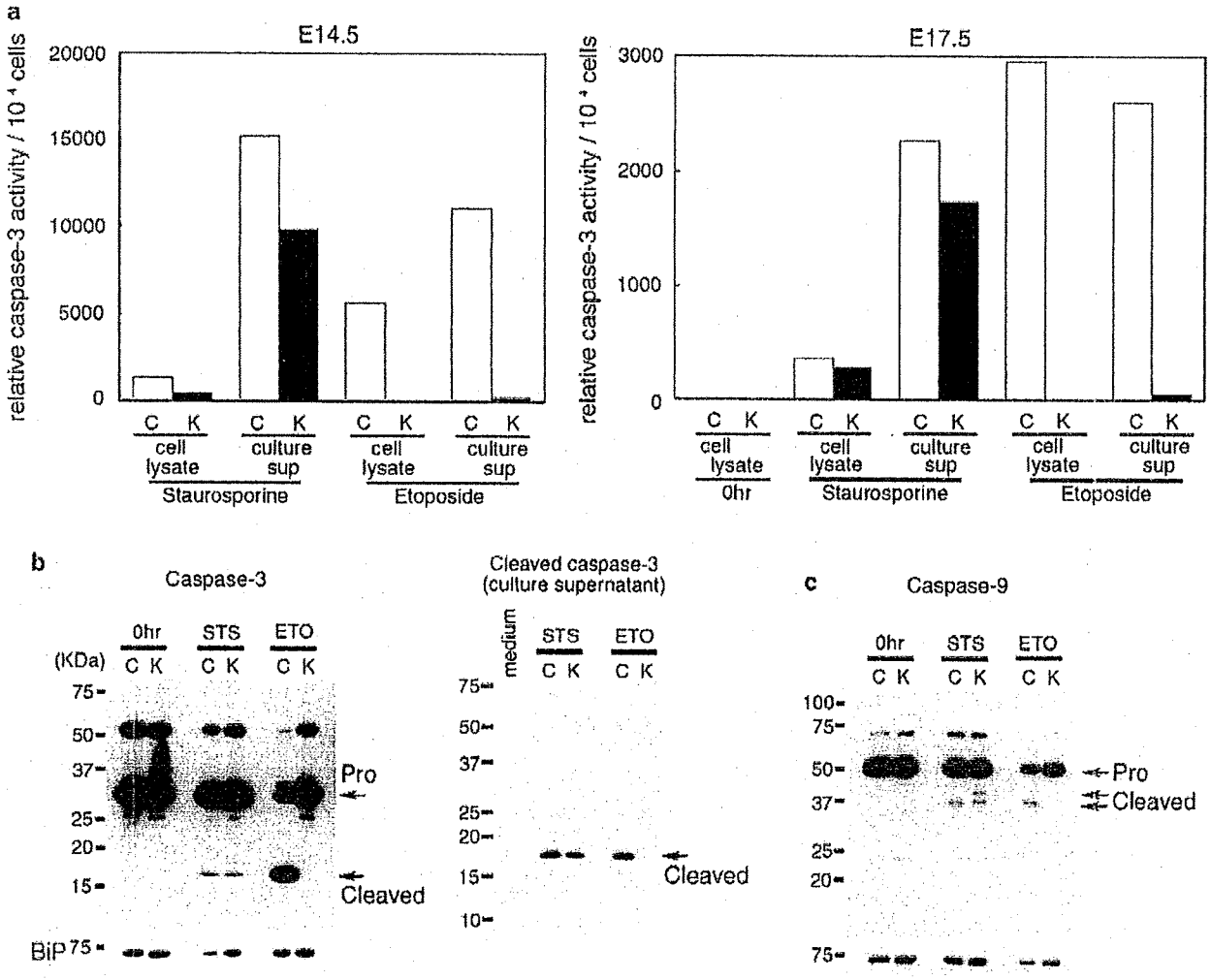

Figure 5 Apaf-1-independent caspase activation. (a) Activation of caspase-3. Thymocytes were prepared from E14.5 or E17.5 embryos with *Apaf-1*$^{+/+}$ or *Apaf-1*$^{+/-}$ (C) and *Apaf-1*$^{-/-}$ (K) genotypes, and treated with 10 μM staurosporine or 50 μM etoposide for 4 h. The caspase activity in the cell lysates and supernatant was determined with Ac-DEVD-AMC as described in Materials and Methods. The caspase activity is expressed in an arbitrary unit. One ng recombinant human caspase-3 gave 14 100 U under the same conditions. Experiments were performed twice with different fetal thymus, and the average values are shown. (b) Processing of caspase-3. In left panel, thymocytes from E17.5 embryos with *Apaf-1*$^{+/+}$ or *Apaf-1*$^{+/-}$ (C) and *Apaf-1*$^{-/-}$ (K) genotypes were treated with 10 μM staurosporine (STS) for 2 h or with 50 μM etoposide (ETO) for 4 h, and the cell lysates were subjected to western blotting with rabbit mAb against mouse caspase-3. The cell lysates from untreated thymocytes were also analyzed (0 h). Bands for the proform and cleaved form of caspase-3 are indicated by arrows. As a loading control, the membrane was re-blotted for BiP, and shown in the bottom. In right panel, thymocytes were treated for 4 h with staurosporine (STS) or etoposide (ETO). The supernatant was immunoprecipitated with rabbit mAb against the cleaved caspase-3, and subjected to western blotting with the same mAb, followed by incubation with HRP-conjugated Protein A. The bands for cleaved caspase-3 are indicated by an arrow. (c) Processing of caspase-9. Thymocytes from E17.5 embryos with *Apaf-1*$^{+/+}$ or *Apaf-1*$^{+/-}$ (C) and *Apaf-1*$^{-/-}$ (K) genotypes were treated 10 μM staurosporine (STS) for 2 h or with 50 μM etoposide (ETO) for 4 h. The cell lysates from the STS- and ETO-treated and untreated (0 h) thymocytes were subjected to western blotting with mouse mAb against mouse caspase-9. Bands for the proform and cleaved form of caspase-9 are indicated by arrows. The membrane was re-blotted for BiP, and is shown in the bottom

similar with those found in other tissues (interdigits, and tail) at E14.5 and 17.5.

Apaf-1-independent caspase activation. To examine whether thymocytes can undergo caspase-dependent apoptotic cell death in the absence of Apaf-1, we prepared thymocytes from the wild-type and *Apaf-1*$^{-/-}$ E14.5 embryos. They were treated with two different apoptosis inducers, etoposide and staurosporine, and the caspase-3 activity in the cell lysates was determined with a fluorescent substrate, Ac-DEVD-AMC. As shown in Figure 5a, a strong caspase-3 activity (about 5600 U) could be detected in the cell lysates from the wild-type but not *Apaf-1*-deficient thymocytes treated with 50 μM etoposide. The cell lysates from the thymocytes treated with 10 μM staurosporine also showed a caspase-3-activity (about 1300 U). Different from the treatment with etoposide, the cell lysates from the staurosporine-treated *Apaf-1*$^{-/-}$ thymocytes carried a significant caspase-3 activity (500 U). The active caspase-3 is often released from the cells into supernatant.[27] In fact, the supernatant from

staurosporine-treated *Apaf-1*$^{+/+}$ and *Apaf-1*$^{-/-}$ thymocytes carried a high caspase-3 activity (10 000–15 000 U). Conversely, the treatment with etoposide produced the caspase-3 activity in the supernatant with *Apaf-1*$^{+/+}$ thymocytes, but not with *Apaf-1*$^{-/-}$ thymocytes. These results indicated that etoposide could activate caspase-3 in E14.5 thymocytes in an Apaf-1-dependent manner, whereas Apaf-1 is dispensable for the staurosporine-induced activation of caspase-3. Similar results were obtained with E17.5 thymocytes, that is, staurosporine but not etoposide activated caspase-3 in E17.5 *Apaf-1*$^{-/-}$ thymocytes as efficiently as *Apaf-1*$^{+/+}$ thymocytes, although the extent of the activated caspase-3 per cell is significantly lower than that found with E14.5 thymocytes (Figure 5a).

To confirm the caspase-3 activity detected with Ac-DEVD-AMC is due to the processed caspase-3, we analyzed the cell lysates using western blot method with the antibody against caspase-3. As shown in Figure 5b, the lysates from the staurosporine-treated *Apaf-1*$^{+/+}$ and *Apaf-1*$^{-/-}$ thymocytes showed a 17 kDa band for the processed caspase-3. This band was detected in the lysates from the etoposide-treated *Apaf-1*$^{+/+}$ but not *Apaf-1*$^{-/-}$ thymocytes, and its intensity correlated with the caspase-3 activity detected (Figure 5a). When the culture supernatants from staurosporine- or etoposide-treated E17.5 *Apaf-1*$^{+/+}$ thymocytes were immunoprecipitated with the antibody against processed caspase-3, they showed the 17 kDa band by western blot with the antibody against the processed caspase-3 (Figure 5b). However, the 17 kDa band was not detected in the immunoprecipitate of the etoposide-treated E17.5 *Apaf-1*$^{-/-}$ thymocytes, which agrees with the little caspase-3 activity in the supernatant (Figure 5a).

In the intrinsic apoptotic pathway, Apaf-1 works as a scaffold to activate caspase-9, which induces processing of procaspase-3.[10] To examine an involvement of caspase-9 in the Apaf-1-independent activation of caspase-3, we carried out western blot analysis with anticaspase-9. As shown in Figure 5c, the 37 kDa processed caspase-9 could be detected in the lysates from the staurosporine-treated *Apaf-1*$^{+/+}$ as well as *Apaf-1*$^{-/-}$ thymocytes. In contrast, the processing of procaspase-9 in the etoposide-treated thymocytes was observed in the *Apaf-1*$^{+/+}$ thymocytes, but not in the *Apaf-1*$^{-/-}$ thymocytes. These results indicate that staurosporine but not etoposide can activate caspase-9 in the absence of Apaf-1.

Discussion

Many cells die during mammalian development. However, as the dead cells are swiftly engulfed by macrophages for degradation, it is difficult to detect them. For example, more than 90% of thymocytes undergo programmed cell death during the development of the thymus. But, only a small percentage of the cells can be stained by TUNEL at a given time point.[28] Many neurons also undergo programmed cell death in the brain, but the reported number differs greatly among researchers,[29–31] probably due to the difficulty in detecting dead cells that are quickly eliminated. Here, we used *DNase II*-null mice to detect the programmed cell death that occurs during mouse embryogenesis. The *DNase II*-null mice carried in various tissues macrophages that contained undigested DNA, suggesting that cells died surrounding the macrophages and were engulfed. Although it is difficult to determine which and how many cells died, the *DNase II*$^{-/-}$ mice were nonetheless useful for localizing the regions where programmed cell death occurs. The macrophages carrying undigested DNA eventually disappeared, probably because those with a heavy load of DNA could not survive, suggesting that the *DNase II*$^{-/-}$ mice can also be used to estimate the time when programmed cell death takes place. In fact, we have been able to show that specific layers of cerebral neurons undergo programmed cell death at specific stages of mouse embryogenesis (AN, KK, and SN, manuscript in preparation).

Crossing the *Apaf-1*$^{-/-}$ mice with *DNase II*$^{-/-}$ mice, we showed that most of the apoptotic cell death during mouse embryonic development takes place through an Apaf-1-dependent pathway. This agrees with previous reports that deletion of the *Apaf-1* or *caspase-9* gene blocks apoptotic cell death in the brain, and ear.[13,14] Similarly, the apoptotic cell death in E17.5 thymus was also blocked by deficiency of *Apaf-1*, indicating that the negative and positive selections at CD4$^+$CD8$^+$ thymocytes proceed in an Apaf-1-dependent pathway. In contrast, very surprisingly, we found that caspase-3 could be activated without Apaf-1 in the E14.5 thymus, in which most thymocytes are CD4$^-$CD8$^-$.[32] Furthermore, staurosporine but not etoposide activated caspase-3 in the fetal thymocytes without Apaf-1. Etoposide and staurosporine are inhibitors for topoisomerase and kinase C, respectively, and both of them have been reported to activate caspase-3 by releasing cytochrome *c* from mitochondria.[33,34] Thus, no requirement of Apaf-1 in the staurosporine-induced activation of caspase-3 in the fetal thymocytes was unexpected. This result suggests that staurosporine can activate caspase-3 in thymocytes through a pathway that does not use cytochrome *c*, and this pathway may be similar to that used in the Apaf-1-independent apoptotic cell death of E14.5 thymocytes. We observed that caspase-3 can be activated without Apaf-1 not only in the fetal thymus but also in the fetal liver (AN, KK, and SN, unpublished observation), which may be consistent with reports that hemopoietic cells reconstituted with fetal liver cells can activate caspase without Apaf-1.[18,35,36] To understand this apoptosis, it will be necessary to determine how and which caspases are activated by staurosporine without Apaf-1.

Even when the caspase was not activated in *Apaf-1*-deficient mice, macrophages carrying undigested DNA were present in the embryo, in particular at the late stage of development, indicating that cells could die without Apaf-1, and were engulfed by macrophages. This agrees with the previous report showing that myeloid cells die without Apaf-1 or caspase-9.[37] Several Apaf-1- or caspase-independent cell death processes have been proposed, including autophagic cell death and necrosis.[38] As reported for the interdigits of *Apaf-1*$^{-/-}$ embryos,[39] we found in the ectodermal ridge of the tails of *Apaf-1*$^{-/-}$ mice many cells exhibiting mottled chromatin condensation, nuclear membrane detachment and rupture, and dilated mitochondria. Whereas, no cells with the characteristics of autophagy (double-membraned vacuoles), indicating that the cells probably died because of necrosis.

One possible cause of nonapoptotic cell death is that the stimuli that induce programmed cell death in mouse embryogenesis cause cytochrome *c* to be released, inactivating mitochondrial function, which leads to cell death.[37] The mice lacking both Bak and Bax that are essential for the release of cytochrome *c*[40] show the persistence of interdigital webs,[17] which suggests that Bak/Bax can cause necrotic cell death by releasing cytochrome *c*. It will be interesting to examine whether the null mutation of *Bax* and *Bak* can prevent the generation of macrophages carrying undigested DNA in *DNase II*-null embryos.

In *Apaf-1*$^{-/-}$ embryos, dead cells were found in macrophages, indicating that the nonapoptotic dead cells were recognized by macrophages for engulfment. In *C. elegans*, a common set of genes mediates the removal of both apoptotic and necrotic cell corpses.[41] Conversely, different mechanisms have been proposed to clear apoptotic and necrotic cells in mammalian system.[42] Apoptotic cells expose phosphatidylserine, which is recognized by specific receptors or opsonins for engulfment.[12] Because necrotic cells also expose phosphatidylserine at a late stage,[38] it is possible that similar receptors or opsonins mediate the engulfment of apoptotic and necrotic cells. The complement system is another candidate for the engulfment of late apoptotic or necrotic cells.[43] It will be interesting to study the engulfment of necrotic cells by crossing the *Apaf-1*$^{-/-}$ mice with mice deficient in the engulfment of apoptotic or necrotic cells.[44,45] Unengulfed apoptotic cells are difficult to find in mouse tissues. However, we frequently detected unengulfed dead cells with nonapoptotic morphology in the *Apaf-1*$^{-/-}$ embryos, suggesting that the engulfment of nonapoptotic dead cells is inefficient compared with that of apoptotic cells. This may allow noxious materials to be released from dying cells. In addition, the engulfment of necrotic cells but not apoptotic ones is known to cause the release of inflammatory cytokines.[46] In this regard, it will be interesting to study whether the normally developing *Apaf-1*$^{-/-}$ mice suffer from inflammatory disease.

Materials and Methods

Mice. C57BL/6 mice were purchased from Nippon SLC (Hamamatsu, Japan) or Shimizu Laboratory (Kyoto, Japan) Supplies. *DNase II*$^{-/-}$ mice[20] were backcrossed to C57BL/6 at lease six times. *IFN-IR*$^{-/-}$ mice[47] in the C57BL/6 background were obtained from Michel Aguet (Swiss Institute for Experimental Cancer Research, Epalinges, Switzerland). *Apaf-1*$^{-/-}$ mice in the C57BL/6 background were described previously.[14,19] *DNase II*$^{-/-}$*IFN-IR*$^{-/-}$ mice and *Apaf-1*$^{-/-}$*DNase II*$^{-/-}$*IFN-IR*$^{-/-}$ embryos were generated by crossing *Apaf-1*$^{+/-}$*DNase II*$^{-/-}$*IFN-IR*$^{-/-}$ parents, respectively. Mice were housed in specific pathogen-free facilities at Osaka University Medical School and Oriental Bio Service. All animal experiments were conducted according to the Guidelines for Animal Experiments of Osaka University or Kyoto University. To determine the genotype of *DNase II* and *IFN-IR* alleles, we prepared DNA from embryonic tissues or adult tail-snip tissue, as described,[48] and analyzed using PCR. For the *DNase II* gene, a sense primer specific for the wild-type (5′-GCCCATCTAGACTAACTTTC-3′) or mutant allele (5′-GATTCGCAGCGCATCG CCTT-3′); sequence in the neomycin-resistant gene) was used with a common antisense primer (5′-GAGTCTTAGTCCTTTGCTCCG-3′). The wild-type and mutant alleles for *IFN-IR* were examined with a wild-type (5′-AAGATGTGCTGTTCCC TTCCTCTGCTCTGA-3′) or mutant-specific (5′-CCTGCGTGCAATCCATCTTG-3′) antisense primer and a common sense primer (5′-ATTATTAAAAGAAAAGACGA GGCGAAGTGG-3′). For the *Apaf-1* allele, a wild-type (5′-CTCAAACACCTCCTCC ACAA-3′) or mutant-specific (5′-GGGCCAGCTCATTCCTC-3′) sense primer was used with a common antisense primer (5′-GTCATCTGGAAGGGCAGCGA-3′).

Histochemical analysis with paraffin sections. Embryos were fixed with 4% PFA in 0.1 M Na-phosphate buffer (pH 7.2) containing 4% sucrose at 4°C for more than 1 day with shaking. They were gradually dehydrated by dipping into 50, 70, 80, and 90% ethanol at room temperature for 12 h each, and then twice in 100% ethanol for 1 h. The samples were soaked twice in 100% xylene at room temperature for 1 h, in a 1 : 1 mixture of xylene and paraffin for 2 h at 60°C. They were embedded in paraffin by successive incubations in paraffin for 12 and 4 h at 60°C, and sectioned at 4 μm using a microtome (RM2245; Leica, Solms, Germany).

For TUNEL staining, sections were treated at room temperature for 20 min with 20 μg/ml Proteinase K, and stained with an Apoptag kit (Millipore, Bedford, MA, USA), according to the manufacturer's instructions, except that the amount of terminal transferase was reduced to 10% of the recommended concentration. Sections were mounted with Mount-Quick (Daido Sangyo, Toda, Saitama, Japan) or Fluoromount (Diagnostic BioSystems, Pleasanton, CA, USA), and observed by fluoroescence microscopy (IX-70; Olympus, Tokyo, Japan or BioRevo BZ-9000; Keyence, Osaka, Japan).

Histochemical analysis with cryosections. Embryos were fixed at 4°C in 4% PFA containing 4% sucrose in 0.1 M Na-phosphate buffer (pH 7.2) for 2 h, successively immersed in 10 and 20% sucrose-containing 0.1 M Na-phosphate buffer (pH 7.2) for 4 h and overnight each, embedded in OCT compound (Sakura Finetek, Tokyo, Japan), and frozen in liquid nitrogen. Sections (10 μm) were prepared using a cryostat (CM3050 S; Leica) in the cold (−16 to −25°C).

To detect active caspase-3, we fixed sections with 4% PFA in PBS at room temperature for 10 min, and blocked with 5% normal goat serum in PBS containing 0.3% Triton X-100 at room temperature for 1 h. They were stained at 4°C overnight with a 100-fold diluted rabbit monoclonal antibody (mAb) against active caspase-3 (clone 5A1E; Cell Signaling, Danvers, MA, USA), followed by incubation at room temperature for 1 h with Cy3-conjugated goat anti-rabbit IgG (Jackson Laboratories, West Grove, PA, USA).

For the staining of F4/80 antigen, a rat hybridoma against mouse F4/80[49] was grown in serum-free GIT medium (Nihon Pharmaceutical, Tokyo, Japan). Cryosections from mouse embryos were fixed at room temperature for 10 min with 1% PFA in PBS. After blocking with 10% normal rabbit serum and 0.5% BSA in PBS at room temperature for 1 h, sections were incubated at 4°C overnight with the supernatant of the F4/80 hybridoma, and washed with PBS containing 0.5% BSA. The endogenous peroxidase was quenched by incubation at 4°C for 20–30 min with 3% H_2O_2 in methanol, and incubated at room temperature for 45 min with peroxidase-conjugated rabbit anti-rat Ig (Dako, Copenhagen, Denmark). The signals were detected by incubation at room temperature for 5 min with Cy3-labeled tyramide (PerkinElmer, Boston, MA, USA).

TUNEL staining was performed as described above, except that the concentration of terminal transferase was reduced to 0.4–0.5% of that recommended by the manufacturer. Sections were mounted with mounting reagent containing 1–2 μg/ml DAPI (Dojin Laboratories, Kumamoto, Japan), and observed by microscopy as described earlier.

Electron microscopy. Embryonic tissues were fixed by incubation at 4°C for 2 h in 0.1 M Na-phosphate buffer (pH 7.2) containing 2% PFA and 2% glutaraldehyde. After being washed five times with 0.1 M Na-phosphate buffer (pH 7.2) at 4°C for 20 min each, the samples were post-fixed at 4°C for 2 h with 1% OsO_4 in the same buffer, and dehydrated at 4°C by dipping into a graded series (50, 60, 70, 80, 90, 99%) of ethanol for 10 min each. After two 20-min immersions in 100% ethanol, the samples were incubated at 35°C twice in propylene oxide for 20 min, in a 3 : 1 mixture of propylene oxide and epoxide for 1 h, in a 1 : 3 mixture of propylene oxide and epoxide for 1 h, and in epoxide overnight. They were then embedded in epoxide by incubation at 60°C for 3 days. Ultrathin sections (80–90 nm) were prepared with an ultramicrotome (Ultracut N; Reichert-Nissei, Kumamoto, Japan), stained with uranyl acetate and lead citrate, and observed with a Hitachi H-7650 microscope (Hitachi High-Technologies, Tokyo, Japan).

Assay for caspase-3. Thymocytes (4×10^4 cells per 100 μl) from E14.5 embryos or thymocytes (5×10^6 cells per 200 μl) from E17.5 embryos were treated with 10 μM staurosporine or 50 μM etoposide in DMEM containing 10% FCS. The caspase-3 activity in the cell lysates and medium was determined using Caspase-3 Cellular Assay Kit PLUS (Enzo Life Sciences, Farmingdale, NY, USA) according to the instructions provided by the manufacturer. In brief, cells were collected by centrifugation at 5000 r.p.m. for 5 min, washed with PBS, and lysed with 50 μl Lysis Buffer (50 mM HEPES-NaOH buffer (pH 7.4), 0.1% CHAPS, 5 mM DTT, and